

# **Yukawa-Type Electro-Weak Corrections to Higgs Boson Pair Production**

Master's Thesis of

Augustin Vestner

at the Department of Physics  
Institute for Theoretical Physics (ITP)

Reviewer:	Gudrun Heinrich
Second reviewer:	Stefan Gieseke
Advisor:	Gudrun Heinrich
Second advisor:	Matthias Kerner

18. Jul 2022 – 18. Jan 2023



---

I declare that I have developed and written the enclosed thesis completely by myself, and have not used sources or means without declaration in the text.

**Karlsruhe, 18.1.2023**

.....  
(Augustin Vestner)



# Abstract

As of now, the Higgs potential is still largely unexplored. To overcome this, a precise knowledge of the Higgs self coupling  $\lambda$  is crucial. Higgs boson pair production in gluon-gluon fusion is one of the most promising processes to measure the self-interaction, since here  $\lambda$  enters already at Born level. However, the leading order (LO) already contains one loop. The calculation of this has been performed already before discovery of the Higgs boson, but at next-to-leading order (NLO) substantial progress has been made in the last decade mainly.

The present work calculates the EW corrections at NLO, focussing on the Yukawa and Higgs self-coupling contributions, while neglecting gauge boson induced corrections. Contrary to previous publications the full top-quark mass dependence is included.

Construction and reduction of the amplitude are performed with `reduze`, the resulting master integrals are evaluated with `pySecDec`. The renormalization is performed employing the Fleischer-Jegerlehner-Tadpole-Scheme. The amplitude is evaluated for a few phase space points.

The renormalization procedure is not yet complete, since at the present state not all poles cancel. Also, the numerical integration takes, despite being run on GPUs, a long time, which prohibits the calculation for many phase space points, as required for phenomenological results. Both issues are subject to further development.

Besides this, a preliminary study of  $gg \rightarrow HH$  mediated by bottom quark loops is presented. It is shown that integrals containing the Higgs as well as the bottom quark mass scale can be evaluated using `pySecDec`. A peek into the effects of varying bottom quark Yukawa couplings on the invariant di-Higgs mass distribution is taken with `POWHEG-BOX`.



# Zusammenfassung

Das Higgspotential ist bisher noch weitestgehend unerforscht. Um diesen Zustand zu ändern, ist die genaue Kenntnis der Higgs Selbstwechselwirkung  $\lambda$  erforderlich. Einer der vielversprechendsten Ansätze ist die Messung der durch Gluonenfusion initiierten Paarproduktion von Higgsbosonen, da hier  $\lambda$  schon in der führenden Ordnung (LO) auftritt. Allerdings enthält selbst diese schon eine Schleife. Die LO Berechnung wurde etliche Jahre vor der Entdeckung des Higgsbosons durchgeführt, doch in der nächst-führenden Ordnung (NLO) wurden hauptsächlich im letzten Jahrzehnt Fortschritte gemacht.

Die vorliegende Arbeit berechnet elektro-schwache Korrekturen in NLO mit einem Fokus auf Yukawa-artigen und Higgsselbstkopplungsbeiträgen, während von den Eichbosonen erzeugte Korrekturen vernachlässigt werden. Anders als bei vorherigen Veröffentlichungen wird die vollständige Topquarkmassenabhängigkeit verwendet.

Die Amplitude wird mit `reduze` erzeugt und reduziert, die resultierenden Masterintegrale werden mit `pySecDec` berechnet. Die Renormalisierung wird unter Nutzung des Fleischer-Jegerlehner-Tadpole-Schemas durchgeführt. An einigen Phasenraumpunkten wird die Amplitude schließlich ausgewertet.

Die Renormalisierung ist noch nicht vollständig abgeschlossen, da sich nicht alle Polestellen aufheben. Ebenfalls benötigt die numerische Integration, trotzdem sie auf GPUs durchgeführt wird, eine sehr lange Zeit, was die Berechnung vieler Phasenraumpunkte, und damit brauchbarer phänomenologischer Ergebnisse, verhindert. Beide Problemstellen unterliegen fortdauernder Entwicklung.

Zusätzlich wird eine vorläufige Untersuchung des Prozesses  $gg \rightarrow HH$ , der durch Bottomquark Schleifen vermittelt wird, vorgestellt. Es wird gezeigt, dass Integrale, die sowohl die Bottomquark-, als auch die Higgsmassenskala beinhalten, mit `pySecDec` berechnet werden können. Die Effekte verschiedener Bottomquark-Yukawa-Kopplungen auf die Verteilung der invariante Masse des Higgs paares wird mit POWHEG-BOX untersucht.

# Contents

<b>Abstract</b>	<b>i</b>
<b>Zusammenfassung</b>	<b>iii</b>
<b>1 Introduction</b>	<b>1</b>
<b>2 The Standard Model of Particle Physics</b>	<b>3</b>
2.1 The General Stage . . . . .	3
2.2 The Higgs Sector and Electro-Weak Symmetry Breaking . . . . .	4
2.3 The Lagrangian in the Scope of This Work . . . . .	8
<b>3 Di-Higgs Production Calculations</b>	<b>11</b>
<b>4 Calculation of Electro-Weak Yukawa and Self-Coupling Corrections</b>	<b>15</b>
4.1 LO Calculation . . . . .	15
4.2 Amplitude Generation . . . . .	17
4.3 Reduction . . . . .	21
4.4 Integration of Master Integrals . . . . .	23
4.5 Renormalization . . . . .	26
4.5.1 Tadpole Renormalization . . . . .	27
4.5.2 Field and Mass Renormalization . . . . .	30
4.5.3 The Renormalized Amplitude . . . . .	34
<b>5 Conclusion and Directions for Further Investigations</b>	<b>37</b>
<b>Bibliography</b>	<b>39</b>
<b>A Appendix</b>	<b>43</b>
A.1 Integrals with Bottom Quark Loops . . . . .	43
A.2 Scalar Integrals and Passarino-Veltman Reduction . . . . .	45
A.2.1 Tensor integral reduction . . . . .	45
A.2.2 Derivative of the Scalar Functions . . . . .	46
A.2.3 Comprehensive Calculations from the Renormalization . . . . .	48



# List of Figures

2.1	Mexican hat potential . . . . .	5
3.1	Higgs pair production cross section . . . . .	12
3.2	LO $H$ pair production diagrams . . . . .	12
3.3	HTL . . . . .	13
4.1	NLO diagrams . . . . .	18
5.1	Gauge field EW correction diagrams . . . . .	37
5.2	$m_{HH}$ distribution including bottom loops . . . . .	38
A.1	Diagrams with bottom loops . . . . .	44

# List of Tables

4.1	Integral families at NLO . . . . .	22
4.2	Additional families in a library . . . . .	22
4.3	Form factor integration results . . . . .	26
A.1	Integrals containing bottom quarks . . . . .	43



# 1. Introduction

The last monumental achievement in particle physics was the experimental confirmation of the Higgs boson's existence in 2012 at the Large Hadron Collider (LHC) at CERN [1, 2], roughly five decades after its prediction by theorists [3–8]. As far as the Standard Model of particle physics (SM) is concerned, the last missing piece was found thereby. The Nobel Prize committee was accordingly impressed and awarded F. Englert and P. Higgs with the Nobel Prize in physics the following year [9].

Luckily, particle physics is far from being a finished field. Even today, more than a decade after its discovery, the Higgs boson remains a mystery. This is to a large extent due to the challenging experimental setups required to measure any of its properties. In fact, finding the Higgs boson was already one of the main goals of the LHC physics programme. Pinning down its properties is a work still in progress. After several cycles of data taking and upgrading the systems, it seems clear that the LHC will never be able to enlighten certain questions, e.g. its self-coupling.

The value of this parameter is crucial for the existence of the universe itself, as it is directly connected to the shape of the Higgs potential. Knowing the precise form of the potential would allow to constrain extended theoretical models beyond the SM (BSM), e.g. models where there are more than one Higgs boson (as super symmetry has it), or models where the Higgs is not a fundamental particle, but a composite, similar to other known scalar particles, like the pions.

Not only improved experiments are required to extend the knowledge. One possibility coming to prominence with the increasing capabilities of modern and post-modern computing clusters is research at the precision frontier. By calculating evermore higher orders in perturbative expansions, effects inaccessible due to experimental energetic limits, can be taken into account indirectly. These theoretical predictions are matched with the simultaneously increasing experimental precision results to derive new bounds in unprecedented parameter regions for BSM physics as well as SM physics.

The present work aims at contributing to exactly this objective, by presenting the calculation of the next-to-leading order (NLO) Yukawa-type electro-weak correction to Higgs pair production from gluon fusion. It starts with an introduction of the SM in chapter 2, elaborates the importance of the  $gg \rightarrow HH$  process in ch. 3, presents the calculation in ch. 4, and closes with an outlook on possible directions of further investigations in ch. 5.



## 2. The Standard Model of Particle Physics

This chapter presents a general introduction to the Standard Model of Particle Physics (SM), containing a more elaborated description of the Higgs sector and the connected electro-weak symmetry breaking (EWSB) in sec. 2.2. The derivation follows mainly ref. [10]. Sec. 2.3 details the simplifications and conventions used during the calculations in ch. 4.

### 2.1. The General Stage

The SM is described by the Lagrangian density [10]

$$\mathcal{L}_{\text{SM}} = \mathcal{L}_{\text{QCD}} + \mathcal{L}_{\text{EW}} , \quad (2.1)$$

which has to obey the gauge symmetry group

$$SU(3)_{\text{color}} \times SU(2)_L \times U(1)_Y . \quad (2.2)$$

The first term concerns quantum chromodynamics (QCD) described in  $\mathcal{L}_{\text{QCD}}$ , the second the electro-weak (EW) sector described in  $\mathcal{L}_{\text{EW}}$ . The Lagrangian can be written out explicitly to show the particle content, namely the Higgs field, the quarks and the leptons, as well as the force fields, namely the photon, the gluons, the  $W$  and the  $Z$  bosons, and all possible interactions amongst them. The force fields emerge directly from the symmetry group as objects in its adjoint representation, while the fermions and the Higgs field live in the fundamental representation regarding the EW sector, see eqs. (2.3), (2.4) and (2.5). In QCD the leptons and the Higgs field are singlets.

QCD is a non-Abelian gauge theory introducing eight bosonic gluons corresponding to the eight generators of  $SU(3)$ . These gluons only interact with particles carrying a colour charge, which are the quarks and the gluons themselves.

The electro-weak sector adds three  $W$  fields from the  $SU(2)$  generators and another  $B$  field from the  $U(1)$  generator. The corresponding charges for these symmetries are the third component of the weak isospin  $I_w^3$  and the hypercharge  $Y$ . These original  $W$  and  $B$  fields are mixed such that the known  $W^\pm$ ,  $Z$  bosons and the photon emerge, and the electric charge  $Q$  is formed, since they carry both colour and electric charge by the mechanism of EWSB.

The leptons and the Higgs field turn up only in the electro-weak part of the Lagrangian, while the quarks are also present in QCD. Left-handed fermions are arranged in doublets of the form

$$\begin{pmatrix} \ell_i \\ \nu_i \end{pmatrix}_L \quad \text{and} \quad \begin{pmatrix} u_i \\ d_i \end{pmatrix}_L \quad (2.3)$$

for leptons and quarks respectively, due to symmetry constraints, whereas the right handed versions are included as singlets

$$\ell_R, u_R \text{ and } d_R . \quad (2.4)$$

The Higgs boson is the only fundamental scalar boson of the theory.

## 2.2. The Higgs Sector and Electro-Weak Symmetry Breaking

The SM Higgs field [10] is realized as the complex  $SU(2)$  doublet

$$\Phi = \frac{1}{\sqrt{2}} \begin{pmatrix} \Phi^+ \\ \Phi^0 \end{pmatrix} , \quad (2.5)$$

therefore containing four degrees of freedom. Its Lagrangian density is

$$\mathcal{L}_\Phi = (D_\mu \Phi)^\dagger (D^\mu \Phi) + \mu^2 \Phi^\dagger \Phi - \frac{\lambda}{4} (\Phi^\dagger \Phi)^2 . \quad (2.6)$$

No higher powers of  $\Phi^\dagger \Phi$  are included, due to renormalizability constraints. For some configurations of  $\mu$  and  $\lambda$  the shape of the potential resembles a sombrero hat, see fig. 2.1, hence it is often called the 'Mexican hat potential'. Due to this particular shape, the minima are not located at the origin, but rather on a circle around it. This causes the Higgs field to have a non-vanishing vacuum expectation value (vev). It can be derived from the Fermi constant as

$$0 \neq \langle \Phi \rangle = v \stackrel{[11]}{=} 246.22 \text{ GeV} . \quad (2.7)$$

It is important to note that the ground state (so to speak in the brim of the hat) is not symmetric any more under the original EW symmetry. This process is referred to as electro-weak symmetry breaking (EWSB). The Lagrangian itself still is symmetric, due to the potential consisting of only even exponents.

The Higgs field can be expanded around the vacuum expectation value (vev), for example as

$$\Phi = \frac{1}{\sqrt{2}} \begin{pmatrix} \phi_1 + i\phi_2 \\ v + H + i\phi_3 \end{pmatrix} \quad (2.8)$$

or

$$\Phi = \frac{1}{\sqrt{2}} \exp \left( i \frac{\phi_i \sigma_i}{v} \right) \begin{pmatrix} 0 \\ v + H \end{pmatrix} , \quad (2.9)$$

where the  $\phi_i$  denote the emerging Goldstone bosons,  $\sigma_i$  the Pauli matrices,  $v$  the vev, and  $H$  the Higgs boson. Using eq. (2.9) the vev can be calculated to be

$$v = \sqrt{\frac{4\mu^2}{\lambda}} . \quad (2.10)$$

It appears in the lower, uncharged component of the doublet, since this component does not carry any charge. Otherwise the vacuum would be charged, thereby violating charge conservation contrary to observation.

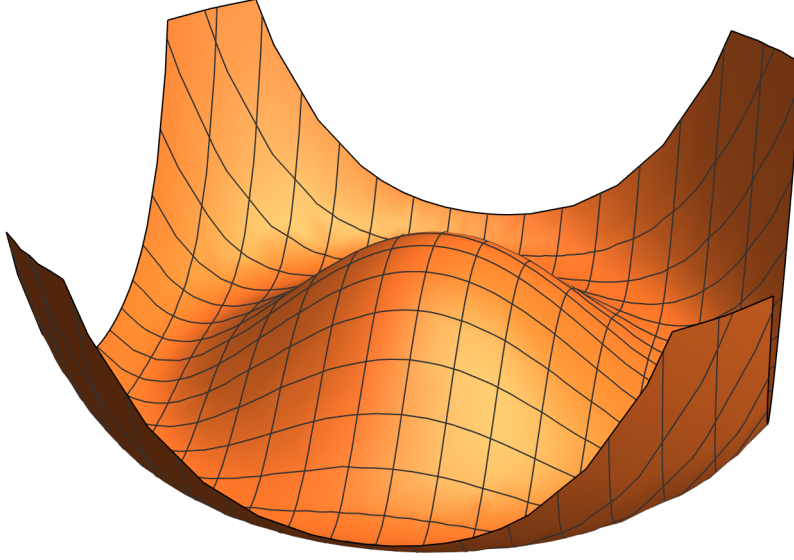


Figure 2.1.: Example of a “mexican hat potential”.

According to the Goldstone theorem [12] every broken generator of the original symmetry group  $SU(2) \times U(1)$  can be associated with a massless scalar boson. Since only the azimuthal  $U(1)$  symmetry of electro-magnetism remains after EWSB, only a single  $U(1)$  generator is left, producing three Goldstone bosons, which carry the remaining degrees of freedom. The Higgs boson is a real scalar field and can therefore carry only one degree of freedom. The three Goldstone bosons are unphysical; this becomes obvious when the unitary gauge is used. In unitary gauge the gauge fixing is performed such that all terms containing Goldstone bosons are eliminated. At the same time the vector bosons  $W^\pm$  and  $Z$  become massive via the covariant derivative of the Higgs doublet.

$$\begin{aligned}
 (D_\mu \Phi)^\dagger (D^\mu \Phi) &= \frac{1}{8} \begin{pmatrix} 0 & v \end{pmatrix} \begin{pmatrix} g'B_\mu + gW_\mu^3 & gW_\mu^1 - igW_\mu^2 \\ gW_\mu^1 - igW_\mu^2 & g'B_\mu + gW_\mu^3 \end{pmatrix} \begin{pmatrix} g'B_\mu + gW_\mu^3 & gW_\mu^1 - igW_\mu^2 \\ gW_\mu^1 - igW_\mu^2 & g'B_\mu + gW_\mu^3 \end{pmatrix} \begin{pmatrix} 0 \\ v \end{pmatrix} \\
 &= \frac{g^2 v^2}{8} \left[ W_\mu^+ W_\mu^- + \left( \frac{g'}{g} B_\mu - W_\mu^3 \right)^2 \right].
 \end{aligned}
 \tag{2.11}$$

Colloquially, physicists say that ‘the vector bosons eat the Goldstone bosons’. Together with a non-zero mass these vector bosons acquire a longitudinal polarization mode. The longitudinal polarizations correspond to the degrees of freedom formerly carried by the Goldstone bosons.

Equation (2.11) introduces the  $W^\pm$  bosons, which are defined as

$$W_\mu^\pm = W_\mu^1 \mp iW_\mu^2.
 \tag{2.12}$$

It is now also possible to define the  $Z$  and  $A$  bosons through the rotation

$$\begin{pmatrix} Z_\mu \\ A_\mu \end{pmatrix} = \begin{pmatrix} c_w & -s_w \\ s_w & c_w \end{pmatrix} \begin{pmatrix} W_\mu^3 \\ B_\mu \end{pmatrix} \quad \Leftrightarrow \quad \begin{pmatrix} B_\mu \\ W_\mu^3 \end{pmatrix} = \begin{pmatrix} c_w & -s_w \\ s_w & c_w \end{pmatrix} \begin{pmatrix} A_\mu \\ Z_\mu \end{pmatrix}, \quad (2.13)$$

where

$$s_w := \sin(\vartheta_w), \quad c_w := \cos(\vartheta_w) \quad \text{and} \quad \tan(\vartheta_w) := \frac{g'}{g}. \quad (2.14)$$

$\vartheta_w$  is the weak mixing angle. Using these definitions it is possible to write

$$\begin{aligned} \left( \frac{g'}{g} B_\mu - W_\mu^3 \right)^2 &= \frac{s_w^2}{c_w^2} (c_w^2 A_\mu A^\mu - 2c_w s_w A_\mu Z^\mu + s_w^2 Z_\mu Z^\mu) \\ &\quad - 2 \frac{s_w}{c_w} (c_w s_w A_\mu A^\mu + (c_w^2 - s_w^2) A_\mu Z^\mu - s_w c_w Z_\mu Z^\mu) \\ &\quad + s_w^2 A_\mu A^\mu + 2s_w c_w A_\mu Z^\mu + c_w^2 Z_\mu Z^\mu \\ &= \frac{1}{c_w^2} Z_\mu Z^\mu = \frac{g^2 + g'^2}{g^2} Z_\mu Z^\mu. \end{aligned} \quad (2.15)$$

Herefrom follows that the photon, denoted by  $A$ , is massless. Combining eq. (2.15) and eq. (2.11) gives a value for the  $Z$  mass of

$$m_Z = \frac{v \sqrt{g^2 + g'^2}}{2} = \frac{m_W}{c_w}. \quad (2.16)$$

Rewriting the whole Lagrangian in terms of the new  $W^\pm$ ,  $Z$  and  $A$  bosons gives the couplings of the Higgs boson to the physical gauge fields. It is then obvious that the coupling strength is proportional to the mass of the coupled vector boson, hence there exist no coupling between the photon and the Higgs boson.

To generate quark masses, Yukawa interaction terms are introduced. Since fermions have mass dimension  $\frac{3}{2}$ , it is possible to construct terms of dimensionality 4 with two fermions and the Higgs field, which has mass dimension 1. The Yukawa Lagrangian then reads

$$\mathcal{L}_{\text{Yuk}} = -y_{ij}^d \bar{Q}_L^i \Phi d_R^j - y_{ij}^u \bar{Q}_L^i \Phi^c u_R^j + \text{h.c.} . \quad (2.17)$$

The  $Q_L$  encodes all left-handed quarks, the  $d_R$  all right-handed down-type quarks, the  $u_R$  all right-handed up-type quarks and the  $\Phi^c$  is the charge conjugated Higgs field

$$\Phi^c = i\sigma_2 \Phi^* . \quad (2.18)$$

Lepton mass terms are included similarly, but due to the right-handed neutrinos being singlets under all SM interactions no Yukawa mass term can be written.

Since the Lagrangian has to be symmetric under the group stated in eq. (2.2), it is in general not possible to have terms of mixed chirality without a  $\Phi$  field in the Yukawa part of the Lagrangian, therefore terms like

$$\mathcal{L}_{\text{evil}} = m_u \bar{Q}_L u_R \quad (2.19)$$



are forbidden: they would change under a  $SU(2)$  transformation, because  $Q_L$  is a doublet and  $u_R$  a singlet.

When the expansion around the vev is inserted for  $\Phi$ , the quark Yukawa terms become

$$\begin{aligned}\mathcal{L}_{\text{Yuk}} &= -\frac{Y_{ij}^d}{\sqrt{2}} (\bar{u}_L^i \quad \bar{d}_L^i) \cdot \begin{pmatrix} 0 \\ v \end{pmatrix} d_R^j - \frac{Y_{ij}^u}{\sqrt{2}} (\bar{u}_L^i \quad \bar{d}_L^i) \cdot \begin{pmatrix} v \\ 0 \end{pmatrix} u_R^j + \text{h.c.} \\ &= -Y_{ij}^d \bar{d}_L^i \frac{v}{\sqrt{2}} d_R^j - Y_{ij}^u \bar{u}_L^i \frac{v}{\sqrt{2}} u_R^j + \text{h.c.} .\end{aligned}\quad (2.20)$$

It is not trivial to see the mass terms for the quarks, since the matrices  $Y^u$  and  $Y^d$  mix different generations. In order to fix this issue, the quarks can be rotated into the *mass basis* via the unitary matrices

$$d_R^i \rightarrow (U_R^d)_{ij} \hat{d}_R^j \quad u_R^i \rightarrow (U_R^u)_{ij} \hat{u}_R^j \quad d_L^i \rightarrow (U_L^d)_{ij} \hat{d}_L^j \quad u_L^i \rightarrow (U_L^u)_{ij} \hat{u}_L^j, \quad (2.21)$$

resulting in the Yukawa matrices becoming diagonal:

$$\hat{M}^d = (U_L^d)^\dagger Y^d U_R^d = \text{diag}(m_d, m_s, m_b) \quad \hat{M}^u = (U_L^u)^\dagger Y^u U_R^u = \text{diag}(m_u, m_c, m_t) \quad (2.22)$$

Inserting these definitions in equation (2.17) yields

$$\begin{aligned}\mathcal{L}_{\text{Yuk}} &= -\frac{v}{\sqrt{2}} \bar{d}_L (U_L^d)^\dagger U_L^d M^d (U_R^d)^\dagger U_R^d d_R - \frac{v}{\sqrt{2}} \bar{u}_L (U_L^u)^\dagger U_L^u M^u (U_R^u)^\dagger U_R^u u_R + \text{h.c.} \\ &= -v M_d^i \bar{d}_L^i d_R^i - v M_u^i \bar{u}_L^i u_R^i + \text{h.c.} .\end{aligned}\quad (2.23)$$

The hat from eqs. (2.21) and (2.22) has been dropped, since all occuring quantities are in the mass basis. The masses for the quarks are given by

$$m_q = \frac{v}{\sqrt{2}} M_q \quad (2.24)$$

with  $M_q$  being the corresponding entry in the diagonal mass matrix.

This rotation also has to take place in the rest of the Lagrangian, namely the kinetic term discussed above. After performing this rotation to the mass basis nearly everywhere the rotation matrices  $U$  drop out. Only the terms where the coupling between  $W^\pm$  and the quarks is described keep the combination

$$V_{\text{CKM}} := (U_L^u)^\dagger U_L^d, \quad (2.25)$$

which is known as the Cabibbo-Kobayashi-Maskawa matrix. This is the source of flavour changing charged currents in the SM and of  $CP$  violation.

As mentioned above the lepton masses are constructed similarly, but due to missing right handed neutrinos in the SM, a similar matrix to the CKM matrix (which would be called Pontecorvo-Maki-Nakagawa-Saki matrix) cannot be constructed within the SM.

It is important to keep in mind that the derivation so far is exclusively in unitary gauge, which is a very specific choice. A more general approach would be to use  $R_\xi$  gauges.

To obtain the unitary gauge the limit  $\xi \rightarrow \infty$  needs to be taken, thereby removing the Goldstone bosons from the particle spectrum. If  $\xi$  is not taken to infinity these unphysical degrees of freedom still exist and also propagate. In order to fix this *ghosts* are introduced (with another extra term to the Lagrangian) to cancel the superfluous degrees of freedom. These ghosts must also be considered when collecting all contributing Feynman diagrams. After performing the calculations, the physical observables must not differ from those obtained in unitary gauge.

### 2.3. The Lagrangian in the Scope of This Work

In the following, only Yukawa and Higgs self interaction vertices will be considered, hence all parts in the Lagrangian corresponding to QCD, gauge bosons, or leptons are neglected, as well as any terms with quarks other than the top, due to their small coupling to the Higgs boson. The Lagrangian can be written as<sup>1</sup>

$$\begin{aligned} \mathcal{L}_{EW,t} = & (D_\mu \Phi)^\dagger (D^\mu \Phi) + i \bar{Q}_L \hat{D} Q_L + i \bar{u}_R \hat{D} u_R \\ & + \mu^2 \Phi^\dagger \Phi - \frac{\lambda}{4} (\Phi^\dagger \Phi)^2 - (y^u \bar{Q}_L \Phi^c u_R + \text{h.c.}) . \end{aligned} \quad (2.26)$$

The first line contains all the kinetic terms needed for a Higgs boson and an up-type quark. The second line contains the biquadratic Higgs potential and the Yukawa coupling. The covariant derivative

$$D_\mu = \partial_\mu - i \frac{g}{\sqrt{2}} W_\mu^a \sigma^a - i \frac{g'}{2} B_\mu \quad (2.27)$$

yields the interaction terms between force and particle fields.  $g$  and  $g'$  are the coupling strengths of the original  $SU(2)_L$  and  $U(1)_Y$  symmetries respectively. The definitions

$$Q_L := \begin{pmatrix} t_L \\ 0 \end{pmatrix}$$

for a left handed and

$$u_R := t_R$$

for a right handed particle are understood. The next simplification is to use unitary gauge, such that

$$\Phi = \frac{1}{\sqrt{2}} \begin{pmatrix} 0 \\ v + H \end{pmatrix} \quad (2.28)$$

with all Goldstone bosons set to zero.

Next the gaugeless limit is taken to get rid of any gauge boson interaction terms. This is done by shifting

$$(g, g') \longrightarrow (0, 0) .$$

Equation (2.27) then loses all gauge boson contributions so

$$D_\mu \longrightarrow \partial_\mu . \quad (2.29)$$

---

<sup>1</sup>The symbol  $\hat{D}$  occuring in eq. (2.26) is an abbreviation of  $\gamma_\mu D^\mu$ , c.f. Feynman slash notation.

Applying all these simplifications to the Lagrangian (2.26) yields

$$\begin{aligned} \mathcal{L}_{\text{EW},t}|_{\text{gaugeless}} = & \frac{1}{2} (\partial_\mu H)^\dagger (\partial^\mu H) + \frac{\mu^2}{2} (v+H)^2 - \frac{\lambda}{16} (v+H)^4 \\ & + i (\bar{t}_L \hat{\partial} t_L + \bar{t}_R \hat{\partial} t_R) - y_t \frac{v+H}{\sqrt{2}} (\bar{t}_L t_R + \text{h.c.}) . \end{aligned} \quad (2.30)$$

The terms containing the top quark fields can be simplified using the anticommutation properties of the gamma matrices and the projection operators:

$$\begin{aligned} \bar{t}_L t_R + \text{h.c.} = & t_L^\dagger \gamma_0 t_R + t_R^\dagger \gamma_0 t_L = t^\dagger P_L \gamma_0 P_R t + t^\dagger P_R \gamma_0 P_L t = t^\dagger \gamma_0 P_R^2 t + t^\dagger \gamma_0 P_L^2 t \\ = & t^\dagger \gamma_0 P_R t + t^\dagger \gamma_0 P_L t = \bar{t} (P_R + P_L) t = \bar{t} t \end{aligned} \quad (2.31)$$

$$\begin{aligned} \bar{t}_R \hat{\partial} t_R + \bar{t}_L \hat{\partial} t_L = & t^\dagger P_R \gamma_0 \gamma_\mu \partial^\mu P_R t + t^\dagger P_L \gamma_0 \gamma_\mu \partial^\mu P_L t = t^\dagger \gamma_0 P_L \gamma_\mu \partial^\mu P_R t + t^\dagger \gamma_0 P_R \gamma_\mu \partial^\mu P_L t \\ = & \bar{t} \hat{\partial} P_R^2 t + \bar{t} \hat{\partial} P_L^2 t = \bar{t} \hat{\partial} (t_R + t_L) = \bar{t} \hat{\partial} t \end{aligned} \quad (2.32)$$

Obtained therefrom is

$$\mathcal{L} = \frac{1}{2} (\partial_\mu H)^\dagger (\partial^\mu H) + \frac{\mu^2}{2} (v+H)^2 - \frac{\lambda}{16} (v+H)^4 + i \bar{t} \hat{\partial} t - y_t \frac{v+H}{\sqrt{2}} \bar{t} t \quad (2.33)$$

$$\begin{aligned} = & \frac{1}{2} (\partial_\mu H)^\dagger (\partial^\mu H) + H v \left( \mu^2 - \frac{\lambda v^2}{4} \right) + H^2 \frac{1}{2} \left( \mu^2 - \frac{3}{4} \lambda v^2 \right) - H^3 \frac{\lambda v}{4} - H^4 \frac{\lambda}{16} \\ & + i \bar{t} \hat{\partial} t - \frac{v y_t}{\sqrt{2}} \bar{t} t - \frac{y_t}{\sqrt{2}} H \bar{t} t . \end{aligned} \quad (2.34)$$

The Lagrangian depends on the parameters  $v$ ,  $\mu$ ,  $\lambda$  and  $y_t$ , which are not independent. Rather  $m_H$ ,  $m_t$  and  $v$  shall be used instead.

To obtain an expression for  $v$  the minimum of the Higgs potential for  $H = 0$  is required, which corresponds to the  $\mathcal{O}(H)$  term in equation (2.34).

$$\left. \frac{\partial V}{\partial H} \right|_{H=0} = \mu^2 - \frac{\lambda v^2}{4} \stackrel{!}{=} 0 \quad \Longrightarrow \quad \lambda = \frac{4\mu^2}{v^2} \stackrel{(2.36)}{=} \frac{2m_H^2}{v^2} \quad (2.35)$$

For the last equality an expression for the Higgs mass is needed, which comes from the bilinear term in the Lagrangian.

$$-\frac{m_H^2}{2} H^2 \stackrel{!}{=} \frac{1}{2} \left( \mu^2 - \frac{3}{4} \lambda v^2 \right) H^2 \stackrel{(2.35)}{=} \left( \mu^2 - \frac{3}{4} \frac{4\mu^2}{v^2} v^2 \right) \frac{H^2}{2} = -2\mu^2 \frac{H^2}{2} \quad \Longrightarrow \quad \mu^2 = \frac{m_H^2}{2} \quad (2.36)$$

Similarly,

$$m_t \bar{t} t \stackrel{!}{=} \frac{v y_t}{\sqrt{2}} \bar{t} t \quad \Longrightarrow \quad y_t = \frac{\sqrt{2} m_t}{v} . \quad (2.37)$$

These expressions will be exploited in sec. 4.5.



### 3. Di-Higgs Production Calculations

As seen previously in equations (2.6) and (2.33), the parameter  $\lambda$  enters the SM on a very fundamental level. It is of the utmost importance, since the shape of the Higgs potential is defined by it, as well as the EWSB mechanism and baryogenesis.

Many new physics models alter the Higgs sector, for instance by considering the Higgs as a composite state. All this would likewise change the form of the potential. To be able to test it for new physics, it is therefore crucial to know the SM Higgs potential shape precisely.

The kappa value allows, within an appropriate effective field theory framework, statements about constraints on SM parameters from measurements. For the parameter  $\lambda$  it is defined as

$$\kappa_\lambda := \frac{\lambda}{\lambda_{\text{SM}}} \quad (3.1)$$

with the expected SM value  $\lambda_{\text{SM}}$ . Similar definitions also hold for other couplings in the SM. The closer a  $\kappa$  value is to 1, the more SM like is the measured value. Right now the value of  $\lambda$  is loosely constrained to be

$$-1.24 \leq \kappa_\lambda \leq 6.4$$

by the CMS experiment [13] and to be

$$-0.4 \leq \kappa_\lambda \leq 6.3$$

by the ATLAS experiment [14], but the high luminosity upgrade of the LHC in immediate future is expected to decrease this interval to

$$0.5 \leq \kappa_\lambda \leq 1.5$$

soon [15]. A physical process featuring the Higgs self coupling is required to decrease the uncertainty on  $\kappa_\lambda$ .

A prime example for such a process is di-Higgs production, which includes  $\lambda$  already at leading order (LO). The cross section plot for  $HH$  production, as seen in fig. 3.1, is quite similar to the one for only single Higgs production but shifted down by three orders of magnitude. It is not surprising to observe the largest production cross section again in the gluon-gluon-fusion (ggF) channel. Vector boson fusion, double Higgs-strahlung, and  $\bar{t}t$  associated pair-production are all at least one order of magnitude smaller. The uncertainties on the gluon fusion production cross section are related to the uncertainties of the self coupling [17] via

$$\frac{\Delta\sigma}{\sigma_{\text{ggF}}} \sim -\frac{\Delta\lambda}{\lambda}.$$

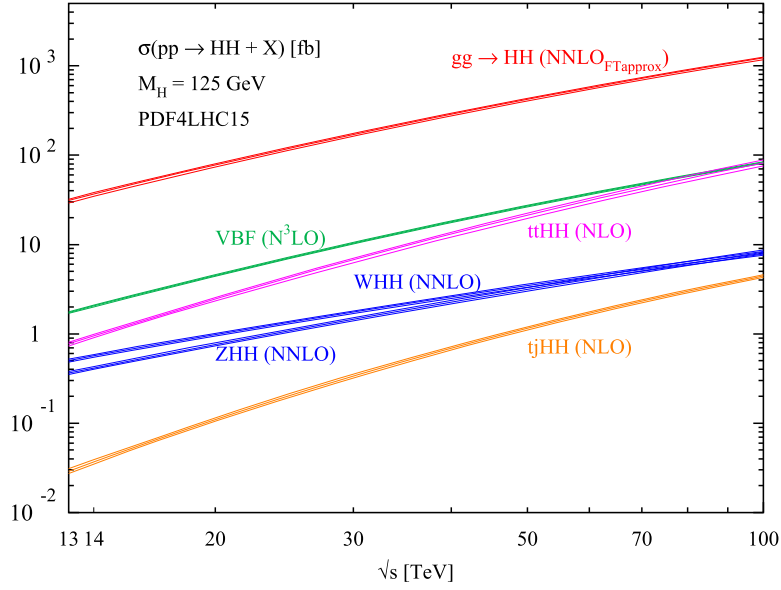


Figure 3.1.: The Higgs pair production cross sections for different production channels as given by [16]. Except for the scale they are very similar to single Higgs production cross sections; again gluon-gluon-fusion dominates.

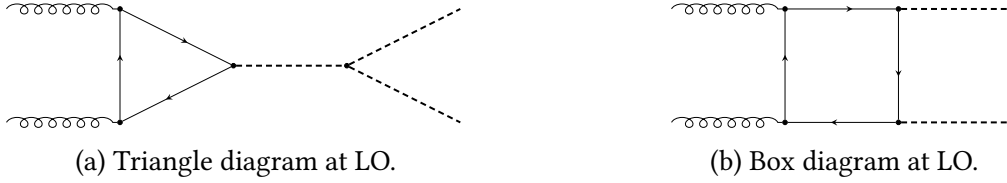


Figure 3.2.: Two LO diagrams contributing to Higgs pair production. Each diagram contains already one loop, since gluons and Higgs bosons do not couple directly. It is obvious that the Higgs self coupling already enters at LO in diagram (a).

It is crucial to minimize the theoretical uncertainties in  $\sigma_{ggF}$ , otherwise the required precision for  $\lambda$  cannot be achieved.

Despite the large cross section compared to the other production channels, the process is quite difficult to measure, because of its small cross section in absolute numbers. Just as with single Higgs production a part of it can be ascribed to the weak coupling between the Higgs and many of the other SM particles, as well as the necessity of loop diagrams already at LO. Moreover, Higgs pair production requires a much higher energy in the partonic process.

Inconveniently, as fig. 3.2 shows, the leading order for  $gg \rightarrow HH$  is already at one loop level. This is a complication, as corrections to the amplitude introduce another loop in the diagrams and the integrals originating are in general not analytically solved yet. Unfortunately, the two LO diagrams also interfere destructively, further diminishing the cross section for Higgs pair production.

Despite the challenges, results in different scenarios are available. QCD corrections already include the complete NLO full top quark mass dependence [18–21]. The additional

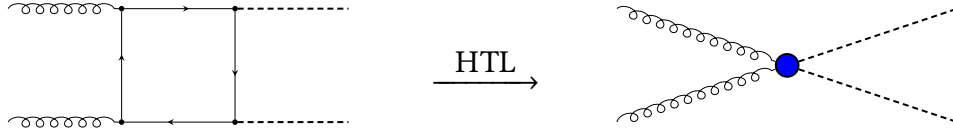


Figure 3.3.: Pictorial representation of the heavy top limit. A top loop becomes an effective coupling.

gluons occurring in higher order diagrams do not introduce another mass-scale to the virtual part. In EW corrections additional Higgs,  $W$ , or  $Z$  bosons in the loops introduce another mass-scale ( $m_H$ ,  $m_W$ , or  $m_Z$  respectively), further complicating the integration. Before the full theory calculations at NLO QCD were achieved, various expansions and approximations were employed. These are nowadays put to use in higher order QCD corrections, and help to address the multiple scales in EW corrections. One of them is the *heavy top limit*<sup>1</sup> (HTL). In this approximation all the top quark loops are integrated out, c.f. fig. 3.3, thereby introducing an effective coupling, reducing the loop order by one, and eliminating one of the mass scales. The NNLO QCD results [22–26] have been computed in this approximation, just as the N<sup>3</sup>LO ggF di-Higgs production calculations [27, 28]. Another approximation is the *Born improved* (BI) cross section. This uses the Born cross section in the full theory  $\sigma_{\text{FT}}$  but rescales it by the normalized NLO corrections in HTL to obtain

$$\sigma_{\text{BI}} = \frac{\mathcal{M}_{\text{HTL}}^{\text{NLO}}}{\mathcal{M}_{\text{FT}}^{\text{LO}}} \sigma_{\text{FT}}. \quad (3.2)$$

This ansatz was used to calculate the NLO QCD corrections [29].

Another next step up the ladder towards a full inclusion of the theory is the *approximated full theory* (FT<sub>approx</sub>). Here everything is calculated with full top quark mass dependence except for virtual corrections, which are calculated in the BI scheme. The authors of ref. [30] obtain their results concerning top quark mass effects in this way.

The unknown EW corrections are assessed to contribute a few percent to the whole cross section with likely larger effects in the tail of the distributions. The EW corrections themselves can still be divided into several branches: one class are corrections induced by the electro-weak bosons  $A$ ,  $W^\pm$  and  $Z$ , another class are the Yukawa induced corrections, containing diagrams with an higher order of Yukawa couplings than the LO diagrams, and yet another class contains higher orders of the Higgs self coupling. Of course, mixtures between those classes are also possible. This thesis is neglecting all corrections from the first kind, which is why the gaugeless limit is taken in sec. 2.3.

Quite recently, a paper [31] by J. Davies, G. Mishima, K. Schönwald, M. Steinhauser, and H. Zhang investigates Yukawa induced corrections in the *high energy limit*. This corresponds to an expansion of the integrands in  $\frac{m_t^2}{s}$ ,  $\frac{m_t^2}{t}$ , and  $\frac{m_t^2}{u}$ . Two different approaches of handling the internal Higgs boson are tested: either as roughly same-scale to the top quark  $m_t^2 \approx (m_H^{\text{intern}})^2$  or very light  $m_t^2 \gg (m_H^{\text{intern}})^2$ .

<sup>1</sup>In some (especially older) references this is called *Higgs effective field theory* (HEFT).

Another recent paper [17] published by M. Mühlleitner, J. Schlenk and M. Spira also investigates the Yukawa induced corrections, but uses the HTL. Here, corrections to the Higgs self coupling are included as well. With this approach they find a  $K$ -factor of

$$K = 1.002$$

with a LO-like trilinear Higgs coupling. The  $K$ -factor quantifies the effect of the higher order correction compared to the so far known order. It is defined as

$$K = \frac{\sigma_{\text{NLO}}}{\sigma_{\text{LO}}} . \tag{3.3}$$



## 4. Calculation of Electro-Weak Yukawa and Self-Coupling Corrections

Section 4.1 reviews the LO calculation as performed by Glover and van der Bij [32]. The NLO calculation is described step by step starting with the amplitude generation in sec. 4.2, continuing with the the integral reduction in sec. 4.3, integration in sec. 4.4, and closing with the renormalization in sec. 4.5.

### 4.1. LO Calculation

The first step is to construct the tensor structure for the  $gg \rightarrow HH$  amplitude. The initial gluons carry a Lorentz index each, since they are vector particles. The final state consists of two Higgs bosons, therefore the matrix element has to be a tensor of rank two in the Lorentz space. It is helpful to divide the amplitude in objects carrying the tensor structure times prefactors, which are known as form factors or structure functions, so

$$\mathcal{M}^{\mu\nu} = \sum_i F_i T_i^{\mu\nu}. \quad (4.1)$$

Considering all possible terms yields an expression

$$\begin{aligned} \mathcal{M}^{\mu\nu} = & a_{00}g^{\mu\nu} + a_{21}p_2^\mu p_1^\nu + a_{31}p_3^\mu p_1^\nu + a_{23}p_2^\mu p_3^\nu + a_{33}p_3^\mu p_3^\nu \\ & + a_{11}p_1^\mu p_1^\nu + a_{22}p_2^\mu p_2^\nu + a_{12}p_1^\mu p_2^\nu + a_{13}p_1^\mu p_3^\nu + a_{32}p_3^\mu p_2^\nu \end{aligned} \quad (4.2)$$

for the amplitude. Due to momentum conservation,  $p_4^\mu$  can be expressed in terms of the other momenta and therefore does not need to be included as additional parameter. The transversal polarization of the gluons restricts the possible terms through the relations

$$\varepsilon_{1,\mu} p_1^\mu = 0 \quad \text{and} \quad \varepsilon_{2,\nu} p_2^\nu = 0. \quad (4.3)$$

This prevents contributions from all terms in the second line of eq. (4.2). Further, restrictions can be derived from the Ward identities

$$p_1^\mu \mathcal{M}_{\mu\nu} = 0 \quad \text{and} \quad p_2^\mu \mathcal{M}_{\mu\nu} = 0. \quad (4.4)$$

Using them gives factors of  $p_1^2 = 0$  or  $p_2^2 = 0$  in some terms, since these momenta are associated with the initial gluons. The Ward identities can be used, since the gluons do not show any non-Abelian behaviour from their  $SU(3)$  group. Here, they behave like photons. The two tensor objects are given by [32]

$$T_1^{\mu\nu} = g^{\mu\nu} - \frac{p_1^\nu p_2^\mu}{p_1 \cdot p_2} \quad (4.5)$$

and

$$T_2^{\mu\nu} = g^{\mu\nu} + \frac{m_H^2 p_1^\nu p_2^\mu}{p_T^2 p_1 \cdot p_2} - \frac{2p_1 \cdot p_3 p_2^\mu p_3^\nu}{p_T^2 p_1 \cdot p_2} - \frac{2p_2 \cdot p_3 p_1^\mu p_3^\nu}{p_T^2 p_1 \cdot p_2} + \frac{2p_3^\mu p_3^\nu}{p_T^2}, \quad (4.6)$$

with the transversal momentum

$$p_T = \sqrt{\frac{\hat{u}\hat{t} - m_H^4}{\hat{s}}}. \quad (4.7)$$

Here, partonic Mandelstam variables are denoted as  $\hat{s}$ ,  $\hat{t}$  and  $\hat{u}$ . Projectors  $\mathcal{P}_i^{\mu\nu}$  are constructed to extract the single form factors, by imposing that

$$\mathcal{P}_i^{\mu\nu} T_{j,\mu\nu} = \delta_{ij}, \quad (4.8)$$

where  $\delta_{ij}$  is the Kronecker delta symbol.

Form factors are gauge- and Lorentz-independent. It is worth noticing that form factor  $F_1$  belongs to the helicity amplitude where both gluons are equally polarized, i.e.  $++$  or  $--$ , whereas  $F_2$  belongs to the helicity amplitude where the gluons have opposite polarization, i.e.  $+-$  or  $-+$ . This shows immediately that triangle diagrams can only contribute to  $F_1$  due to their rotational symmetry around the axis given by the Higgs propagator. The box diagrams on the contrary, contribute to both form factors. In particular

$$F_1(\triangle) = \frac{12m_H^2 m_t^2}{\hat{s} - m_H^2} (2 + (4m_t^2 - \hat{s}) C(p_1, p_2)), \quad (4.9)$$

$$\begin{aligned} F_1(\square) = & 4m_t^2 \left[ m_t^2 (8m_t^2 - \hat{s} - 2m_H^2) (D(p_1, p_2, p_3) + D(p_2, p_1, p_3) + D(p_1, p_3, p_2)) \right. \\ & + \frac{\hat{u}\hat{t} - m_H^4}{\hat{s}} (4m_t^2 - m_H^2) D(p_1, p_3, p_2) + 2 + 4m_t^2 C(p_1, p_2) \\ & \left. + \frac{2}{\hat{s}} (m_H^2 - 4m_t^2) ((\hat{t} - m_H^2) C(p_1, p_3) + (\hat{u} - m_H^2) C(p_2, p_3)) \right] \end{aligned} \quad (4.10)$$

and

$$\begin{aligned} F_2(\square) = & 2m_t^2 \left[ 2 (8m_t^2 + \hat{s} - 2m_H^2) [m_t^2 (D(p_1, p_2, p_3) + D(p_2, p_1, p_3) + D(p_1, p_3, p_2)) \right. \\ & \left. - C(p_3, p_4)] - 2 [\hat{s} C(p_1, p_2) + (\hat{t} - m_H^2) C(p_1, p_3) + (\hat{u} - m_H^2) C(p_2, p_3)] \right. \\ & + \frac{1}{\hat{u}\hat{t} - m_H^4} [\hat{s}\hat{u} (8\hat{u}m_t^2 - \hat{u}^2 - m_H^4) D(p_1, p_2, p_3) + \hat{s}\hat{t} (8\hat{t}m_t^2 - \hat{t}^2 - m_H^4) D(p_2, p_1, p_3) \\ & + (8m_t^2 + \hat{s} - 2m_H^2) [\hat{s} (\hat{s} - 2m_H^2) C(p_1, p_2) + \hat{s} (\hat{s} - 4m_H^2) C(p_3, p_4) \\ & \left. \left. + 2\hat{t} (m_H^2 - \hat{t}) C(p_1, p_3) + 2\hat{u} (m_H^2 - \hat{u}) C(p_2, p_3) \right] \right] \end{aligned} \quad (4.11)$$

for the triangle ( $\triangle$ ) and box ( $\square$ ) type diagram contributions [32]. The gluon momenta are  $p_1$  and  $p_2$ , the Higgs boson momenta are  $p_3$  and  $p_4$ . The functions

$$C(p_1, p_2) = \int \frac{d^4 l}{i\pi^2} \frac{1}{(l^2 - m_t^2)((l + p_1)^2 - m_t^2)((l + p_1 + p_2)^2 - m_t^2)} \quad (4.12)$$

and

$$D(p_1, p_2, p_3) = \int \frac{d^4 l}{i\pi^2} \frac{1}{(l^2 - m_t^2)((l + p_1)^2 - m_t^2)} \times \frac{1}{((l + p_1 + p_2)^2 - m_t^2)((l + p_1 + p_2 + p_3)^2 - m_t^2)} \quad (4.13)$$

are scalar integrals in  $D = 4$  dimensions<sup>1</sup>.

## 4.2. Amplitude Generation

Just as with the LO calculation, the first step at NLO is to determine the contributing diagrams. For EW corrections only additional Yukawa-like and Higgs self-couplings are considered; additional gluon lines would contribute to QCD corrections. Furthermore, only virtual corrections, i.e. additional internal lines, are possible, since real corrections (initial or final state radiation or additional particle radiation from the loop) would change the process from  $gg \rightarrow HH$  to something else, e.g.  $gg \rightarrow HHH$ . This has the great advantage that the calculation of the diagrams is greatly simplified, since no real emission need to be considered and therefore all integrals and the amplitude must be IR finite<sup>2</sup>.

QGRAF [33] is used to automatically generate all contributing Feynman diagrams. A few examples are shown in fig. 4.1. As can be seen, planar as well as non-planar integral contribute. It needs a few files which define the properties of the used physics model. In the present case the EW sector of the SM. Once this is completed, a configuration script is created. In it the model, the loop order, conventions for the momenta, output style, particles to be considered and a flock of other options is specified.

All external momenta are set to be incoming. The momentum conservation law reads

$$0 = p_1 + p_2 + p_3 + p_4 \quad \Leftrightarrow \quad p_4 = -p_1 - p_2 - p_3, \quad (4.14)$$

and the Mandelstam variables are

$$s = (p_1 + p_2)^2, \quad t = (p_1 + p_3)^2 \quad \text{and} \quad u = (p_2 + p_3)^2. \quad (4.15)$$

Some of the diagrams, as, for example, the lower two, are non-planar.

Two different approaches to generate the form factors are used. The first method consists of using a library [34], a Mathematica library, developed to facilitate the connection of

<sup>1</sup>Here, at LO,  $D = 4$  can be used, since the corresponding scalar integrals in  $D = 4 - 2\epsilon$  dimensions are finite.

<sup>2</sup>Integrals without divergences from the integration momentum approaching zero are called IR-finite.

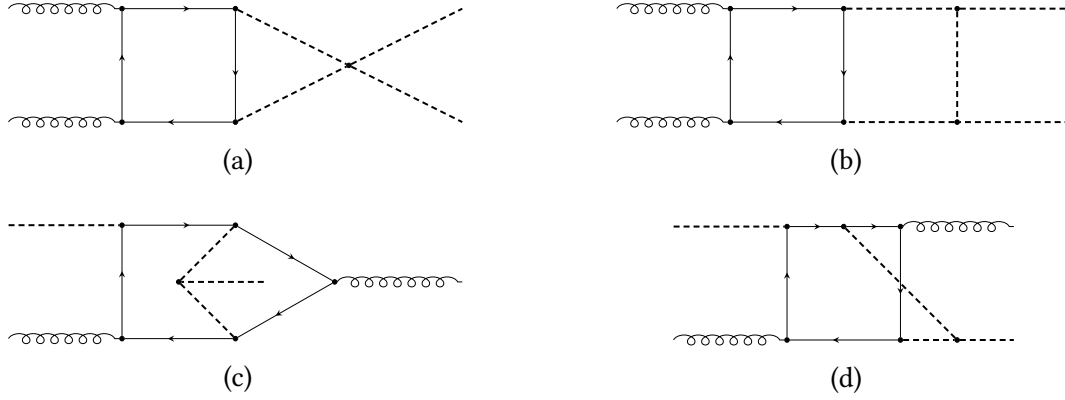


Figure 4.1.: Subset of diagrams considered for NLO EW corrections. The diagrams (c) and (d) are non-planar.

the several programs needed in the computation. `alibrary` provides a model and a style file for QGRAF and interacts through a python wrapper script with it. The default model needs to be adapted to accommodate Higgs self-interaction. QGRAF returns a `.m` file, the content of which must be adapted to the direction of momenta and the elimination of  $p_4$  by eq. (4.14).

Afterwards, the amplitude is constructed from the diagrams using a Mathematica function contained in `alibrary` and multiplied by the projectors to get the form factors. The projectors used here are

$$P_1^{\mu\nu} = \frac{i}{4(d-3)} \delta_{ab} \left\{ (d-2) \left( g^{\mu\nu} - \frac{p_1^\nu p_2^\mu}{p_1 \cdot p_2} \right) + (4-d) \left[ g^{\mu\nu} + \frac{1}{2(p_1 \cdot p_3) \frac{p_2 \cdot p_3}{p_1 \cdot p_2} - m_H^2} \cdot \right. \right. \\ \left. \left. \cdot \left( 2p_3^\mu p_3^\nu + \frac{m_H^2 p_1^\nu p_2^\mu - 2(p_1 \cdot p_3) p_2^\mu p_3^\nu - 2(p_2 \cdot p_3) p_1^\nu p_3^\mu}{p_1 \cdot p_2} \right) \right] \right\} \quad (4.16)$$

and

$$P_2^{\mu\nu} = \frac{i}{4(d-3)} \delta_{ab} \left\{ (4-d) \left( g^{\mu\nu} - \frac{p_1^\nu p_2^\mu}{p_1 \cdot p_2} \right) + (d-2) \left[ g^{\mu\nu} + \frac{1}{2(p_1 \cdot p_3) \frac{p_2 \cdot p_3}{p_1 \cdot p_2} - m_H^2} \cdot \right. \right. \\ \left. \left. \cdot \left( 2p_3^\mu p_3^\nu + \frac{m_H^2 p_1^\nu p_2^\mu - 2(p_1 \cdot p_3) p_2^\mu p_3^\nu - 2(p_2 \cdot p_3) p_1^\nu p_3^\mu}{p_1 \cdot p_2} \right) \right] \right\}. \quad (4.17)$$

The  $a$  and  $b$  indices are adjoint  $SU(3)_{\text{color}}$  indices. A normalization factor of

$$(\delta_{ab} \delta^{ab} - 1)^{-1} = \frac{1}{N_c^2 - 1} = \frac{1}{8} \quad (4.18)$$

for the colours is included later in eq. (4.29).

The next step consists of extracting the list of denominators (containing loop momenta), which can be directly used by the interface to `kira` [35–37] after minor transformations; one of the options for the IBP reduction programs (c.f. sec. 4.3). This is feasible at LO. At NLO the amplitude proved to be too complicated to be reduced by the automated interface. Here, the reduction is performed by another IBP reduction program named `reduze` [38], for further details see sec. 4.3. Hence, `kira` is not used and therefore another way of generating the amplitude is followed.

The second method used to generate the amplitude, which is followed here, is via `reduze`. `reduze` also contains interfaces to some other programs typically used in particle physics calculations, even though its main focus is the IBP reduction. One of them is, again, `QGRAF`: a style file is provided, so that `reduze` may be able to convert the diagrams generated by `QGRAF` into integral expressions. `QGRAF` still needs to be run separately as described above, but everything else is automated within `reduze`. The only thing left to do is to configure `reduze`. In general, `reduze` takes a *job file* as input. This file defines all actions `reduze` takes during the run. Other important files are contained in the required directory `config`. The file `kinematics.yaml` contains all the conventions for the momenta as well as kinematic invariants, i.e. the used names of the Mandelstam variables and particle masses, and scalar products of the external momenta.

The file `feynmanrules.yaml` contains all the rules for diagrams to be converted to mathematical expressions. The projectors from eqs. (4.16) and (4.17) need to be defined here as well. The coupling constants are kept general to be  $g_{HH}$  for triple-Higgs vertex,  $g_{H^3}$  for four-Higgs vertex and  $g_{Ht}$  for top-Higgs-interaction.

The third necessary file is `integralfamilies.yaml`. The Feynman diagrams are translated to integrals for the calculation and those integrals all belong to certain classes. As a matter of fact, each integral is defined by the type and power of occurring propagators in the integrand, and admits the general representation

$$I(v_i) = \int \prod_{l=1}^L \frac{d^D k_l}{(2\pi)^{D/2}} \frac{1}{P_1^{v_1} \dots P_t^{v_t} P_{t+1}^{v_{t+1}} \dots P_n^{v_n}}, \quad (4.19)$$

where the propagators  $P_i$  read

$$P = \left( \sum_i \alpha_i l_i + \sum_i \beta_i p_i \right)^2 - m^2 \quad (4.20)$$

with loop momenta  $l_i$ , external momenta  $p_i$  and the particle mass  $m \geq 0$ . The indices  $L$  and  $n$  in eq. (4.19) give the number of loops and the number of propagators respectively. The number of propagators in an integral family is fixed by the fact that all scalar products containing at least one loop momentum have to be unambiguously expressed through a linear combination of propagators; so there must be

$$\#_P = E \cdot L + \frac{1}{2}L(L-1) \quad (4.21)$$

propagators with the number of legs  $E$  and the number of loops  $L$ . The exponents  $v_i$  with  $i > t$ ,  $0 \leq t \leq n$  are negative to allow construction of momenta in the numerator. At

two-loop level Feynman diagrams for gluon-gluon fusion initiated di-Higgs production exhibit up to seven internal lines, each of which gives rise to a distinct denominator. Two additional, auxiliary denominators are needed to allow the construction of every possible scalar product, as required. `integralfamilies.yaml` describes all integral families for the specified loop order. Each family is defined by a name, the names of the loop momenta and a list of nine propagators. The families can be constructed from the observed diagrams or from similar processes with already known families, but whenever a family is missing, `reduze` issues a message, so that the file content can be extended.

To generate the amplitude, first the `reduze job setup_sector_mappings` is run to check for symmetries between different sectors of the integral families. A sector is defined by propagators in eq. (4.19) with a positive, non-zero exponent. Many sectors are either zero or can be expressed as a linear combination of other sectors. Some are related by symmetries, for example a shift of momenta. In this way, all zero or redundant sectors can be skipped in the next steps.

Second, the job `find_diagram_shifts` is called. This translates the diagrams generated by QGRAF to integral expressions. The integrals are expressed in form of specific sectors of the integral families, by specifying the family name and the vector  $\vec{v}$  of propagator exponents; other information – like the sector number, the number of positive exponents  $t$  and the number of inverted propagators, i.e. negative exponents,  $s$  – can all also be derived therefrom. The sectors vary a lot in complexity and this job tries to match the diagrams to the least complicated ones.

Following this, the job `compute_diagram_interference` introduces interferences between the diagrams to account for cancellations and finally the jobs `sum_terms`, `normalize` and `collect_integrals` allow to finalize the construction of the amplitude. `sum_terms` just adds up terms given as input, whilst `normalize` simplifies the acquired expressions by applying symmetries, shifts and normalization. `collect_integrals` creates a list of all the integrals contained in the output of the job `normalize`. This is not necessary for the amplitude itself, but is necessary to process the loop integrals.

At all times, it is possible to export generated files to a Mathematica format, where they can be processed further. In principle the amplitude is now available, but since the next step – reduction – is also performed with `reduze`, the results are not yet exported.

Both ways of generating the amplitude were implemented at LO, but due to the fact that the NLO computation needs a far more complicated reduction than the automation of the `kira` interface in `alibrary` could handle, the first ansatz was abandoned.

### 4.3. Reduction

The mathematical expressions arising from the diagrams contain many integrals. To a large extent it is not (yet) possible to calculate them analytically, so they need to be evaluated numerically. Performing numerical integration to a high precision can be very time-consuming. In order to decrease the number of integrals, a mathematical trick is employed: integration-by-parts (IBP) reduction. The algorithm is described in ref. [39] by S. Laporta, on account of which it is colloquially referred to as *Laporta algorithm*. The method uses integration by parts to find dependencies between various integrals. It is based on the fact that integrals of total derivatives are zero in dimensional regularization [40].

$$\int \prod_{l=1}^L d^D k_l \frac{d}{dk_i^\mu} [\eta^\mu \mathcal{I}(\vec{\eta})] = 0 \quad (4.22)$$

with  $\eta$  any linear function of internal or external momenta and  $\mathcal{I}$  an integrand as in eq. (4.19). From every integral a number of equations can be built with this technique, generating an system of equations. A Gaussian algorithm can now be used to eliminate as many integrals as possible from the amplitude. The comparatively small set of remaining integrals called *master integrals* needs to be integrated numerically. Another set of equations used to reduce the integrals are the Lorentz-invariance identities. They do not introduce new information, but help speeding up the calculations [40].

There is a certain freedom in the choice of the master integrals and it is critical to choose them wisely. Both the reduction speed and the complexity of the final expression for the amplitude strongly depend on it. If it turns out that the chosen basis is not ideal, *reduze* allows for a change of basis without the need to go through the whole reduction process again. One criterion is that the basis *D-factorizes*. This means that the integrand can be represented as a product of a polynomial depending only on the dimensionality  $D$  (and therefore the regularization parameter  $\epsilon$ ) and one depending only on kinematic variables. *reduze* is able to swap momenta within an integral family to generate the corresponding *crossed* families. For example, a family F1x12 is constructed by exchanging the momenta  $p_1$  and  $p_2$  whenever they turn up in family F1.

At LO the whole amplitude is reduced to eight master integrals. The NLO expression is by far more complicated, hence the reduction needs considerably more time and computing resources. Due to this, the NLO reduction has been performed and contributed by Matthias Kerner. The families used in the reduction can be found in tab. 4.1.

A peculiarity of the setup arises from the fact that *reduze* is able to create the crossed versions of the families, but *kira* does not. As *alibrary* is intended for use with *kira*, it cannot handle the crossed families returned by *reduze*. Another complication is given by integrals with an integration dimension differing from  $4 - 2\epsilon$ . In the current case one integral with a reduced integration dimension of  $2 - 2\epsilon$  (denoted by an appended *dimdec2* to the family name) is present. To overcome these complications, nine additional auxiliary integral families F8 through F14 are introduced, see tab. 4.2, where the corresponding changes are hard-coded in the definition of the family.

The reduction can be performed using either fixed values for  $m_H$  and  $m_t$  or by keeping them symbolic. The latter has the advantage, that at a later stage the masses could be

Table 4.1.: Integral families used in the reduction (up to permutations of the external legs). reduce automatically constructs crossed versions, for alibrary they are manually entered as additional families 8 through 14, c.f. tab. 4.2.

F1	F2	F3	F4
$l_1^2 - m_t^2$	$l_1^2 - m_t^2$	$l_1^2 - m_H^2$	$l_1^2 - m_t^2$
$l_2^2 - m_t^2$	$l_2^2 - m_t^2$	$(l_1 - l_2)^2 - m_t^2$	$l_2^2 - m_H^2$
$(l_1 - l_2)^2 - m_H^2$	$(l_1 - l_2)^2 - m_H^2$	$(l_1 + p_1)^2 - m_t^2$	$(l_1 - l_2)^2 - m_t^2$
$(l_1 + p_1)^2 - m_t^2$	$(l_1 + p_1)^2 - m_t^2$	$(l_2 + p_1)^2 - m_t^2$	$(l_1 + p_1)^2 - m_t^2$
$(l_2 + p_1)^2 - m_t^2$	$(l_2 + p_1)^2 - m_t^2$	$(l_1 - p_2)^2 - m_H^2$	$(l_2 + p_1)^2 - m_H^2$
$(l_1 - p_2)^2 - m_t^2$	$(l_1 - p_3)^2 - m_t^2$	$(l_2 - p_2)^2 - m_t^2$	$(l_1 - p_2)^2 - m_t^2$
$(l_2 - p_2)^2 - m_t^2$	$(l_2 - p_3)^2 - m_t^2$	$(l_2 - p_2 - p_3)^2 - m_t^2$	$(l_2 - p_2)^2 - m_H^2$
$(l_1 - p_2 - p_3)^2 - m_t^2$	$(l_1 - p_2 - p_3)^2 - m_t^2$	$(l_1 + p_1 + p_3)^2 - m_H^2$	$(l_1 - p_2 - p_3)^2 - m_t^2$
$(l_2 - p_2 - p_3)^2 - m_t^2$	$(l_2 - p_2 - p_3)^2 - m_t^2$	$(l_2 + p_1 - p_2)^2 - m_H^2$	$(l_2 - p_2 - p_3)^2 - m_H^2$

F5	F6h	F7h
$l_1^2 - m_H^2$	$l_1^2 - m_H^2$	$l_1^2 - m_t^2$
$l_2^2 - m_t^2$	$l_2^2 - m_t^2$	$l_2^2 - m_t^2$
$(l_1 - l_2)^2 - m_t^2$	$(l_1 - l_2)^2 - m_t^2$	$(l_1 - l_2)^2 - m_H^2$
$(l_1 + p_1)^2 - m_H^2$	$(l_1 - p_3)^2 - m_H^2$	$(l_1 + p_1)^2 - m_t^2$
$(l_2 + p_1)^2 - m_t^2$	$(l_2 - p_3)^2 - m_H^2$	$(l_2 + p_1)^2 - m_t^2$
$(l_1 - p_3)^2 - m_H^2$	$(l_2 + p_2)^2 - m_t^2$	$(l_1 - p_2)^2 - m_t^2$
$(l_2 - p_3)^2 - m_t^2$	$(l_1 + p_1 + p_2)^2 - m_H^2$	$(l_2 - p_2)^2 - m_t^2$
$(l_1 - p_2 - p_3)^2 - m_H^2$	$(l_1 - l_2 + p_1)^2 - m_t^2$	$(l_1 - l_2 + p_3)^2 - m_H^2$
$(l_2 - p_2 - p_3)^2 - m_t^2$	$(l_1 - l_2 - p_2 - p_3)^2 - m_H^2$	$(l_2 - p_2 - p_3)^2 - m_t^2$

Table 4.2.: Translation of the reduce syntax family names to the alibrary names. x indicates the crossing of the momenta following the x, dimdec indicates a reduction of the integration dimension by the number following the dimdec.

reduce	F1	F1dimdec2	F1x12	F2	F2x12	F3	F4
alibrary	B1	B2	B3	B4	B5	B6	B7

reduce	F4x12	F5	F5x12	F6h	F6hx12	F7h	F7hx12
alibrary	B8	B9	B10	B11	B12	B13	B14



exchanged for other values, e.g. including a bottom quark instead of a top quark, but the disadvantage of being more challenging for the reduction procedure. In the present case the ratio of the two masses is fixed according to

$$\frac{m_H^2}{m_t^2} \equiv \frac{12}{23} . \quad (4.23)$$

This is an approximation of the measured values with the advantage of being composed of integers. This reduces floating point errors in numerical calculations.

It is possible that the basis used here is not optimal. A hint in this direction is the long time needed to evaluate the master integrals, see sec. 4.4. In principle an optimal basis should also be quasi-finite, i.e. the divergencies should be factorized to the prefactor. After the reduction is performed, the reduced amplitude is imported into a Mathematica notebook. For the next steps, a list of all master integrals, a list of their coefficients, and the propagators associated with each family are extracted from it.

## 4.4. Integration of Master Integrals

Finally, the integration of the master integrals is performed with pySecDec, as described in refs. [41–43]. pySecDec is a software implementing the semi-analytical sector decomposition method from refs. [44, 45].

In multi-loop calculations integrals are in general divergent, either for high values of the loop momenta (ultraviolet divergence, UV) or for values around zero (infrared divergence, IR). In order to evaluate these integrals numerically, those divergences need to be subtracted. A subtraction procedure describes the splitting of the integral into one summand carrying the pole and one summand consisting of the finite part of the integral still to be integrated, see ref. [45] for a formal description. As long as the singularities are all separated from each other, subtraction is straightforward. However, in higher orders the pole structure is often so complicated that the naïve schemes do not work.

The canonical example [45] is the following integral

$$\mathfrak{I} = \int_0^1 dx \int_0^1 dy x^{-1-a\varepsilon} y^{-b\varepsilon} (x + (1-x)y)^{-1} ; \quad (4.24)$$

the integrand is simultaneously diverging for  $x \rightarrow 0$  and  $y \rightarrow 0$ . Sector decomposition is then applied in two steps. The first step consists of multiplying the integrand with a conveniently chosen factor of 1.

$$\mathfrak{I} = \int_0^1 dx \int_0^1 dy x^{-1-a\varepsilon} y^{-b\varepsilon} (x + (1-x)y)^{-1} [\Theta(x-y) + \Theta(y-x)] . \quad (4.25)$$

Now, a variable transformation  $y = xt$  in the first and  $x = yt$  in the second summand is performed.

$$\mathfrak{I} = \int_0^1 \frac{dx}{x^{1+(a+b)\varepsilon}} \int_0^1 \frac{dt}{t^{b\varepsilon} (1 + (1-x)t)} + \int_0^1 \frac{dx}{y^{1+(a+b)\varepsilon}} \int_0^1 \frac{dt}{t^{1+a\varepsilon} (1 + (1-y)t)} \quad (4.26)$$

and both limits  $x \rightarrow 0$  and  $y \rightarrow 0$  are independent.

In particle physics the integration variables will often be Feynman parameters, and the expressions are in general not so easy that the poles factor performing a single division of the integration region. Rather, the algorithm needs to be iterated several times, until all overlapping infinities are separated. In principle one can proceed as described above for each of the emerging sub-sectors<sup>3</sup>.

pySecDec is built upon an earlier tool of name SecDec, see ref. [46], programmed to a large part in C++. In addition to several feature enhancements, a python and a C++ interface are supplied.

To compute the master integrals, first the sector-decomposed expression for the amplitude and the integrals is generated, and then the numerical integration for a specific phase space point takes place. For pySecDec usage, all the integrals and their prefactors are defined at first. This is done through a python script. Interpreting that script generates several C++ files, which produce the executable once compiled. The executable takes a phase space point as input and returns its value as a series expansion in  $\varepsilon$ .

In the present calculation, the `alibrary` interface to pySecDec is relied on to transfer the kinematic invariants and conventions from `reduze` to pySecDec by `Mathematica`. The integration files can be generated in two ways. On the one hand, the `alibrary` function `SecDecPrepareSum` can be used for each of the form factors separately. It takes a list of all integrals to be evaluated, a list of their coefficients, and a list of *bases* as input. Then it constructs a `compile.py` file, which defines all integrals in a syntax compatible with pySecDec by usage of its `LoopPackage`, and all corresponding coefficients by usage of its `Coefficient` function. Additionally, this file contains a call for the `sum_package` function from pySecDec, which contains the instructions on how to combine all integrals with each other to receive the full form factor back. The order of the  $\varepsilon$  expansion and the real parameters, like the Higgs and top quark mass, can be specified. Additionally, a `Makefile` and a script `integrate.py` are created. All of this is done for each form factor separately, which in principle introduces unnecessary duplications of code, since the master integrals are almost exactly the same for both form factors and would hence be needed to be evaluated only once. The difference lies in the different prefactors multiplying the master integrals.

The other option is to use again the `sum_package`, providing a nested list for the integrals and the coefficients, where the sub-lists correspond to the respective form factors. However, when testing this method for the LO case, the expansion in  $\varepsilon$  showed an unexpected behaviour, the origin of which is not yet clear. To avoid introducing any errors, this method is discarded at present.

At LO, the form factor  $F_1$  requires the evaluation of eight master integrals, whereas for  $F_2$  only a subset of seven is needed. The additional master integral in  $F_1$  is of triangle type, since box diagrams contribute to both form factors, but triangle type diagrams only to  $F_1$  (see sec. 4.1). Similarly, at NLO  $F_1$  contains 496 master integrals, one of which is missing in  $F_2$ . At NLO, the expressions for the coefficients grow very large. In order to handle them properly, it is helpful to substitute the values for the masses  $m_H$  and  $m_t$  from the very

---

<sup>3</sup>Further details can be found in ref. [45].

beginning. To further facilitate the numerical evaluation of the integrals, the rescaling

$$m_t \equiv 1 \quad (4.27)$$

is applied. According to the squared-mass ratio of eq. (4.23) the Higgs mass becomes

$$m_H \approx 0.722315 . \quad (4.28)$$

These numerical values are substituted in the form factors. In the case of NLO, the `compile.py` files created by `SecDecPrepareSum` are  $\sim 4$  GB large.

This script generates a directory containing a subdirectory for each master integral with the C++ source code files. The file `integrate_sum.cpp` defines the integration routine and the construction of the expression for the form factor, storing all adjustable parameters for the integrator of choice. This can be used to adjust the requested relative precision order by order in  $\epsilon$ . The relative precision is the ratio of the uncertainty on the value over the value itself. In the basis used for the reduction at NLO,  $\epsilon$  poles down to  $\epsilon^{-4}$  occur, even though only  $\epsilon^{-1}$  poles are non-spurious. The terms of spurious poles must cancel each other. Requesting a too high relative precision for the prefactors is computationally inefficient<sup>4</sup>. Therefore the relative precision for the spurious orders is set to 100, whereas the orders  $\epsilon^{-1}$  and  $\epsilon^0$  are requested at a relative uncertainty of  $1 \times 10^{-3}$  for form factor  $F_1$  and of  $5 \times 10^{-3}$  for form factor  $F_2$ . The difference is due to the fact that the integration of  $F_2$  takes way longer, so a smaller relative precision is used to reduce the integration time.

The code is now compiled to produce numerical results. The executable program should be run on graphical processing units (GPUs) for time optimization. Compiling for GPUs requires the usage of the `nvcc` compiler, instead of the usual `g++`. Moreover, parallelization to multiple threads greatly decreases integration time. All of this has to be carried out separately for each form factor.

The compilation returns the executable `integrate_sum`. Calling it like

```
./integrate_sum <mH> <mT> <s> <t>
```

on a GPU with actual values substituted for the masses and kinematic variables returns a result for the form factor as a series expansion in  $\epsilon$  up to the requested order. This allows to check whether spurious poles cancel or not.

As input a set of points distributed according to the Born-level cross-section, generated by M. Kerner for a previous project, is used. All points are rescaled to match the top mass from eq. (4.27).

For two phase space points the integration is executed to validate the program. Tab. 4.3 lists the results, omitting the spurious poles. For some phase-space regions the integration converges, as the first point shows, but in others, as the second point proves, it does not. Possibly, this is due to the complexity of the integrals, with several non-planar contributions. Also the integration usually takes several days. At the present state the program is not feasible to integrate large sets of phase-space points, as required for phenomenological

<sup>4</sup>The zero will already be represented by a very small number and the uncertainty on this zero must be an even smaller number, which is readily a numerical fiasco.

Table 4.3.: Results for the integration of the algorithm validation phase space points.  $\sigma_{F_i}$  denotes the uncertainty on the specified order and  $T(F_i)$  shows the time required for the integration in hours.  $s$  and  $t$  are rescaled according to (4.27). The second validation point shows non-convergent behaviour.

$s$	6.392	5.709
$t$	-1.038	-4.597
$O(1)$ of $F_1$	-278.3 + i495.6	-15011.6 - i901.57
$O(1)$ of $\sigma_{F_1}$	-5.8 - i36.1	26053.1 + i25813.5
$O(\varepsilon^{-1})$ of $F_1$	866.55 + i235.91	873.495 + i120.488
$O(\varepsilon^{-1})$ of $\sigma_{F_1}$	10.7971 - i15.6292	3.86608 + i3.81091
$O(1)$ of $F_2$	-5.8 - i36.1	-54908.3 + i108288
$O(1)$ of $\sigma_{F_2}$	0.19 + i0.17	516882 + i554901
$O(\varepsilon^{-1})$ of $F_2$	10.7971 - i15.6292	57320.7 + i12899
$O(\varepsilon^{-1})$ of $\sigma_{F_2}$	0.014 + i0.016	27729.6 + i38457.8
$T(F_1)/h$	45	163
$T(F_2)/h$	347	131

results. With a better suited basis for the master integrals this behaviour might be improved.

The values for the form factors are now combined to get the value of the amplitude through

$$\mathcal{A} = \frac{\alpha_s^2 G_F^2}{8^2 \cdot 256\pi^2} (|F_1|^2 + |F_2|^2) , \quad (4.29)$$

where  $\alpha_s$  is the strong coupling constant and  $G_F$  the Fermi constant. The correction factor  $1/8$  is included to account for the colour structure.

## 4.5. Renormalization

The concept of renormalizability is of great importance in field theories. As stated in sec. 2.2 the Higgs potential contains no higher powers than  $(\Phi^\dagger \Phi)^2$ , due to renormalizability constraints.

To illustrate the problem consider the 1-loop correction to the photon propagator [10],

$$\text{wavy line} \text{---} \text{circle} \text{---} \text{wavy line} \sim \int d^4k \frac{k^2}{k^4} \sim \int k dk = \infty \quad (4.30)$$

with loop momentum  $k$ . A singularity cannot occur in the real world, but luckily the Lagrangian itself is only an intermediate state in the calculation, and is not a observable by itself. It is then possible to extend it by adding *counterterms*. These counterterms are chosen such that they exactly cancel all infinities during the calculation, so in the end, when calculating observables, finite results are obtained. The prescriptions defining how the counterterms are calculated are called renormalization conditions.

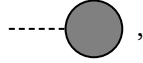
Counterterms appear, when parameters and fields in the Lagrangian are redefined to

be the *bare* quantities, which can be expressed by a combination of counterterms and renormalized quantities. This is done order by order, which is why this procedure is known as *renormalized perturbation theory*.

To get a full renormalization of the amplitude for Higgs boson pair production at NLO EW in the gaugeless limit, the renormalization of  $v$  via the Fleischer-Jegerlehner-Tadpole-Renormalization-Scheme (FJTS) (see sec. 4.5.1) and then the renormalization of fields and masses (see sec. 4.5.2) is needed.

#### 4.5.1. Tadpole Renormalization

Tadpole renormalization is required, whenever higher order corrections in EW theories are calculated. The idea is that  $v$  is not necessarily the true minimum of the Higgs potential, but rather only for a given perturbative order. Hence at the next order the Higgs field is not expanded around its true vev, but around a slightly off value. Therefore, in addition to the usual higher order diagrams, also tadpoles, like



need to be taken into account. The blob includes all possible structures at all loop orders. Only tadpoles with a Higgs leg need to be considered here, since tadpoles with a top leg do not exist in the SM. The complete renormalization procedure is iteratively performed order by order, c.f. [47].

The process is started at LO by determining the Higgs mass and the vev, as in eqs. (2.36) and (2.35):

$$m_H^2 = \frac{3}{4}\lambda v^2 - \mu^2 = 2\mu^2 \quad \text{and} \quad v = \sqrt{\frac{4\mu^2}{\lambda}}.$$

Nothing else needs to be done, since the Higgs field is actually expanded around its true minimum: all tadpole diagrams include at least one loop and are hence relevant only at higher perturbative orders.

The renormalization condition for tadpole renormalization is that the renormalized one-point function  $\Gamma_{1\text{PI}}^H$  vanishes [47]

$$\Gamma_R^H = \Gamma_{1\text{PI}}^H + \delta t = T^H + \delta t = 0, \quad (4.31)$$

which in turn yields

$$\delta t = -T^H. \quad (4.32)$$

$\delta t$  is the tadpole counterterm and  $T^H$  are the Higgs-legged tadpole diagrams.

At NLO  $\delta t$  is not zero and to calculate its value the FJTS [48] either introduces the shift

$$H_0 \longrightarrow H_0 + \Delta v \quad (4.33)$$

or, before fixing the vev, the shift

$$v \longrightarrow v + \Delta v. \quad (4.34)$$

The Lagrangian from eq. (2.33) becomes

$$\mathcal{L} = \frac{1}{2} (\partial_\mu H)^\dagger (\partial^\mu H) + \frac{\mu^2}{2} (v + \Delta v + H)^2 - \frac{\lambda}{16} (v + \Delta v + H)^4 + i\bar{t}\hat{\partial}t - y_t \frac{v + \Delta v}{\sqrt{2}} \bar{t}t - \frac{y_t}{\sqrt{2}} H \bar{t}t . \quad (4.35)$$

After the expansion of the brackets, this reads

$$\begin{aligned} \mathcal{L} = & \frac{1}{2} (\partial_\mu H_0)^\dagger (\partial^\mu H_0) + i\bar{t}\hat{\partial}t - \left( \frac{y_t v}{\sqrt{2}} + \Delta v \frac{y_t}{\sqrt{2}} \right) \bar{t}t - \frac{y_t}{\sqrt{2}} H \bar{t}t \\ & + \left[ \frac{\mu^2 v^2}{2} - \frac{\lambda v^4}{16} + \Delta v \left( \mu^2 v - \frac{v^3 \lambda}{4} \right) + \Delta v^2 \left( \frac{\mu^2}{2} - \frac{3v^2 \lambda}{8} \right) - \Delta v^3 \left( \frac{v \lambda}{4} \right) - \Delta v^4 \left( \frac{\lambda}{16} \right) \right] \\ & + H \left[ \mu^2 v - \frac{\lambda v^3}{4} + \Delta v \left( \mu^2 - \frac{3}{4} \lambda v^2 \right) - \Delta v^2 \left( \frac{3}{4} \lambda v \right) - \Delta v^3 \left( \frac{\lambda}{4} \right) \right] \\ & + H^2 \left[ \frac{\mu^2}{2} - \frac{3}{8} \lambda v^2 - \Delta v \left( \frac{3}{4} \lambda v \right) - \Delta v^2 \left( \frac{3}{8} \lambda \right) \right] \\ & - H^3 \left[ \frac{\lambda}{4} v + \Delta v \left( \frac{\lambda}{4} \right) \right] \\ & - H^4 \left[ \frac{\lambda}{16} \right] . \end{aligned} \quad (4.36)$$

All terms of order  $\Delta v^2$  are not required at NLO and will be omitted. The renormalization condition of eq. (4.31) is constructed using the  $O(H)$  terms, giving

$$-T^H = \mu^2 v - \frac{\lambda v^3}{4} + \Delta v \left( \mu^2 - \frac{3}{4} \lambda v^2 \right) . \quad (4.37)$$

Comparing these terms to the LO expressions, one finds that the first two terms must be equal to zero, whereas the part within brackets is identified with the unrenormalized Higgs mass, resulting in

$$\delta t = -\Delta v m_H^2 \quad \Leftrightarrow \quad \Delta v = -\frac{\delta t}{m_H^2} \quad (4.38)$$

for the tadpole counterterm. The contribution of the tadpole correction to other quantities can then be extracted. The Higgs mass receives the correction

$$\Delta m_H^2 = 2 \left[ \underbrace{\frac{3}{8} \lambda v^2 - \frac{\mu^2}{2}}_{\stackrel{(2.36)}{=} m_H^2/2} + \Delta v \frac{3}{4} \lambda v \right] - m_H^2 = \frac{3}{2} \lambda v \Delta v , \quad (4.39)$$

as follows from the  $O(H^2)$  term. This yields

$$\Delta m_H^2 := \frac{3}{2} \cdot \left( \frac{2m_H^2}{v} \right) \cdot \left( -\frac{\delta t}{m_H^2} \right) = -\frac{3\delta t}{v} . \quad (4.40)$$

The three-Higgs counterterm reads

$$\Delta_{H^3} := \frac{\lambda v}{4} + \frac{\lambda}{4} \Delta v - c_{H^3} = \frac{\Delta v \lambda}{4} = -\frac{\delta t}{2v^2}. \quad (4.41)$$

Finally, the top mass counterterm reads

$$\Delta m_t := \frac{y_t v}{\sqrt{2}} + \Delta v \frac{y_t}{\sqrt{2}} - m_t = \Delta v \frac{y_t}{\sqrt{2}} = -\frac{m_t}{m_H^2 v} \delta t. \quad (4.42)$$

To obtain the expressions for the counterterms all that is left to do is to calculate  $\delta t = -T^H$ , i.e. all the Higgs-legged tadpole diagrams. There are two of them at 1-loop level: one containing a top loop and one containing a Higgs loop.

The top loop tadpole gives

$$\begin{aligned} \text{---} \bigcirc \text{---} &\stackrel{[49]}{=} - \sum_{\text{colours}} i \frac{g}{2} \frac{m_t}{m_W} (-1) \int \frac{d^D l}{(2\pi)^D} \text{Tr} \left[ \frac{i(\hat{l} + m_t)}{l^2 - m_t^2} \right] = -\frac{N_c m_t}{v} \int \frac{d^D l}{(2\pi)^D} \frac{D \cdot m_t}{l^2 - m_t^2} \\ &= -D \cdot N_c \cdot \frac{m_t^2}{v} A_0(m_t). \end{aligned} \quad (4.43)$$

$A_0$  denotes the scalar integral

$$A_0(m) = \mu^{4-D} \int \frac{d^D l}{(2\pi)^D} \frac{1}{l^2 - m^2} \stackrel{[50]}{=} \frac{\Gamma^2(1-\varepsilon)\Gamma(1+\varepsilon)}{\Gamma(1-2\varepsilon)} \frac{i}{2^D \pi^{D/2}} m^2 \left( \frac{\mu^2}{m^2 - i0} \right) (\varepsilon^{-1} + 1) + \mathcal{O}(\varepsilon) \quad (4.44)$$

in  $D$  dimensions, where  $N_c$  is the number of colours and  $\mu^{D-4}$  a correction factor to stay consistent with the mass scale. It is possible to take the limit  $D \rightarrow 4$  without any problems, since the integral is finite in  $D = 4 - 2\varepsilon$  dimensions.

The Higgs loop tadpole is evaluates to

$$\begin{aligned} \text{---} \bigcirc \text{---} &\stackrel{[49]}{=} -i \frac{3g}{4} \frac{m_H^2}{m_W} \mu^{D-4} \int \frac{d^D l}{(2\pi)^D} \frac{i}{l^2 - m_H^2} = \frac{3m_H^2}{2v} \mu^{D-4} \int \frac{d^D l}{(2\pi)^D} \frac{1}{l^2 - m_H^2} \\ &= \frac{3m_H^2}{2v} A_0(m_H). \end{aligned} \quad (4.45)$$

The Feynman rules used here can be found in ref. [49]. The  $W$  boson mass is removed via the relation

$$m_W = \frac{1}{2} g v. \quad (4.46)$$

The counterterm is the negative of the sum of the two diagrams of eqs. (4.43) and (4.45)

$$\delta t = D N_c \cdot \frac{m_t^2}{v} A_0(m_t) - \frac{3m_H^2}{2v} A_0(m_H). \quad (4.47)$$

The FJTS introduces tadpole counterterms via the shift of either the Higgs field or the vev. The inclusion of all tadpoles in the calculation would be therefore equivalent. A huge benefit of this scheme is that all the mass and coupling counterterms are gauge independent. Another advantage is that the tadpole counterterm cancels all tadpole sub-diagrams; this property will be of use in subsection 4.5.2.

### 4.5.2. Field and Mass Renormalization

After the tadpole renormalization, the Lagrangian takes the form

$$\begin{aligned} \mathcal{L} = & \frac{1}{2} (\partial_\mu H_0)^\dagger (\partial^\mu H_0) + i \bar{t}_0 \hat{\partial} t_0 - \left( m_{t,0} - \frac{m_t}{m_H^2 v} \delta t \right) \bar{t}_0 t_0 - \frac{m_{t,0}}{v} H_0 \bar{t}_0 t_0 + \text{const.} \\ & + H \delta t - H_0^2 \left( \frac{m_{H,0}^2}{2} - \frac{3\delta t}{2v} \right) - H_0^3 \left( \frac{m_{H,0}^2}{2v} - \frac{\delta t}{2v^2} \right) - H_0^4 \frac{m_{H,0}^2}{8v^2}, \end{aligned} \quad (4.48)$$

where the index 0 denotes bare quantities, while renormalized quantities have no index. Note that neither  $v$ , which was renormalized in the last subsection, nor any quantity in a term together with  $\delta t$  displays an index, since  $\delta t$  already contains higher order effects. The counterterms are defined by fixing the relation between bare and renormalized quantities to

$$H_0 = \sqrt{Z_H} H \approx \left( 1 + \frac{1}{2} \delta Z_H \right) H, \quad (4.49)$$

$$t_0 = \sqrt{Z_t} t \approx \left( 1 + \frac{1}{2} \delta Z_t \right) t, \quad (4.50)$$

$$m_{H,0}^2 = m_H^2 + \delta m_H^2, \quad (4.51)$$

$$m_{t,0} = m_t + \delta m_t. \quad (4.52)$$

Substituting these in eq. (4.48) gives

$$\begin{aligned} \mathcal{L} = & \frac{1}{2} \left( 1 + \frac{1}{2} \delta Z_H \right)^2 (\partial_\mu H)^\dagger (\partial^\mu H) + i \left( 1 + \frac{1}{2} \delta Z_t \right)^2 \bar{t} \hat{\partial} t - \left( 1 + \frac{1}{2} \delta Z_t \right)^2 \left( m_t + \delta m_t - \frac{m_t}{m_H^2 v} \delta Z_t \right) \bar{t} t \\ & - \frac{m_t + \delta m_t}{v} \left( 1 + \frac{1}{2} \delta Z_H \right) \left( 1 + \frac{1}{2} \delta Z_t \right)^2 H \bar{t} t + \text{const.} + \delta t H \\ & - \left( 1 + \frac{1}{2} \delta Z_H \right)^2 \left( \frac{m_H^2 + \delta m_H^2}{2} - \frac{3\delta t}{2v} \right) H^2 - \left( 1 + \frac{1}{2} \delta Z_H \right)^3 \left( \frac{m_H^2 + \delta m_H^2}{2v} - \frac{\delta t}{2v^2} \right) H^3 \\ & - \left( 1 + \frac{1}{2} \delta Z_H \right)^4 \frac{(m_H^2 + \delta m_H^2)}{8v^2} H^4 \end{aligned} \quad (4.53)$$

$$\begin{aligned} = & \frac{1}{2} (\partial_\mu H)^\dagger (\partial^\mu H) + i \bar{t} \hat{\partial} t - m_t \bar{t} t - \frac{m_t}{v} H \bar{t} t - H^2 \frac{m_H^2}{2} - H^3 \frac{m_H^2}{2v} - H^4 \frac{2m_H^2}{v^2} + \text{const.} \\ & + \frac{\delta Z_H}{2} (\partial_\mu H)^\dagger (\partial^\mu H) + i \delta Z_t \bar{t} \hat{\partial} t - \left( m_t \delta Z_t + \delta m_t - \frac{m_t \delta t}{m_H^2 v} \right) \bar{t} t \\ & - \frac{1}{v} \left( \delta m_t + \frac{m_t}{2} \delta Z_H + m_t \delta Z_t \right) H \bar{t} t + \delta t H - \left( m_H^2 \delta Z_H + \delta m_H^2 - \frac{3\delta t}{v} \right) \frac{H^2}{2} \\ & - \left[ \frac{1}{2v} \left( \delta m_H^2 + \frac{3m_H^2}{2} \delta Z_H \right) - \frac{\delta t}{2v^2} \right] H^3 - \frac{1}{8v^2} (\delta m_H^2 + 2m_H^2 \delta Z_H) H^4. \end{aligned} \quad (4.54)$$



Again, all terms containing higher than linear orders of counterterms are omitted. The first line of eq. (4.54) is the known Lagrangian with renormalized quantities instead of bare ones. The next two lines give the counterterm insertions for the propagators and vertices. Their Feynmanrules are

$$\text{---}\star\text{---} = i \left[ \delta Z_H p^2 - \left( m_H^2 \delta Z_H + \delta m_H^2 - \frac{3\delta t}{v} \right) \right], \quad (4.55)$$

$$\text{---}\star\text{---} = i \left[ \hat{p} \delta Z_t - \left( m_t \delta Z_t + \delta m_t - \frac{m_t \delta t}{m_H^2 v} \right) \right], \quad (4.56)$$

$$\begin{array}{c} \text{---} \\ \diagup \quad \diagdown \\ \star \end{array} = -\frac{i}{v} \left( \delta m_t + \frac{m_t}{2} \delta Z_H + m_t \delta Z_t \right), \quad (4.57)$$

$$\begin{array}{c} \text{---} \\ \diagup \quad \diagdown \\ \star \\ \diagup \quad \diagdown \\ \text{---} \end{array} = -i3 \left[ \frac{1}{v} \left( \delta m_H^2 + \frac{3m_H^2}{2} \delta Z_H \right) - \frac{\delta t}{v^2} \right], \quad (4.58)$$

$$\begin{array}{c} \text{---} \\ \diagup \quad \diagdown \\ \star \\ \diagup \quad \diagdown \\ \text{---} \end{array} = -i \frac{3}{v^2} (\delta m_H^2 + 2m_H^2 \delta Z_H) \quad (4.59)$$

This is in agreement with the counterterms, as found by [47].

In the vertex insertions the top-quark field renormalization is actually not needed; the reason being that each top-leg of any vertex comes with a top-quark field renormalization factor of  $\sqrt{Z_t}$ , whereas each propagator (i.e. inverse two-point function) comes with a factor of  $Z_t^{-1}$ , so for all internal particles these contributions cancel. For the given process top-quarks only occur in the loop. Hence, the only field renormalization required is the one for the Higgs, which also appears as an external particle, see also sec. 4.5.3.

**Top quark renormalization** Considering the top quark two-point function up to NLO, one finds

$$\begin{aligned} G_t(\hat{p}) &= \text{---} + \text{---} \text{---} \text{---} \text{---} + \text{---} \star \text{---} \quad (4.60) \\ &= \frac{1}{\hat{p} - m} + \frac{i}{\hat{p} - m} \Sigma_2(\hat{p}) \frac{i}{\hat{p} - m} + \frac{i}{\hat{p} - m} \left[ \hat{p} \delta Z_t - \left( m_t \delta Z_t + \delta m_t - \frac{m_t \delta t}{m_H^2 v} \right) \right] \frac{i}{\hat{p} - m}. \end{aligned}$$

The first term is the LO part, which is just the propagator, then all the one particle irreducible (1PI) loop contributions to the self-energy  $\Sigma_2(\hat{p})$  follow, and finally the counterterm insertion from eq. (4.56) is included. The latter is also a NLO effect. If this series would be expanded by further 1PI subdiagrams a geometric series would emerge, c.f. [10]. It is common to include all higher order corrections to the self-energy in the definition of

$$\Sigma_t(\hat{p}) = \Sigma_2(\hat{p}) + (\hat{p} - m_t) \delta Z_t - \delta m_t + \frac{m_t \delta t}{m_H^2 v} + \dots \quad (4.61)$$

with the higher orders denoted by the dots. Therefrom follows the form

$$G_t(\hat{p}) = \frac{1}{\hat{p} - m_t + \Sigma_t(\hat{p})} \quad (4.62)$$

for the two-point function. At this stage, the renormalization scheme has to be decided on. A common choice is the *on-shell* scheme. It requires the pole of a particles propagator to be exactly at its renormalized mass. In formulae, this is written as [10]

$$0 = \left[ \Sigma_t(\hat{p}) \right]_{\hat{p}=m_t} \quad \text{and} \quad 0 = \left[ \frac{d}{d\hat{p}} \Sigma_t(\hat{p}) \right]_{\hat{p}=m_t}. \quad (4.63)$$

These two conditions fix the remaining counterterms  $\delta m_t$  and  $\delta Z_t$ .

Before eq. (4.63) can be processed, the expression for  $\Sigma_2(\hat{p})$  is needed. For the top quark only the sunrise diagram with a Higgs contributes to NLO. This is

$$\begin{aligned} \Sigma_2(\hat{p}) &= \text{---}\overset{\curvearrowright}{\text{---}} \stackrel{[49]}{=} \left(-i\frac{m_t}{v}\right)^2 \mu^{D-4} \int \frac{d^D l}{(2\pi)^D} \frac{i(\hat{p} + \hat{l} + m_t)}{(p+l)^2 - m_t^2} \cdot \frac{i}{l^2 - m_H^2} \\ &= \frac{m_t^2}{v^2} \cdot \left[ (\hat{p} + m_t) B_0(p, m_H, m_t) + \mu^{D-4} \gamma_\mu \int \frac{d^D l}{(2\pi)^D} \frac{l^\mu}{(l^2 - m_H^2)((p+l)^2 - m_t^2)} \right] \\ &\stackrel{(A.19)}{=} \frac{m_t^2}{v^2} \cdot \left( m_t + \frac{m_t^2 - m_H^2 + p^2}{2p^2} \hat{p} \right) B_0(p, m_H, m_t) + \frac{m_t^2 \hat{p}}{2p^2 v^2} [A_0(m_H) - A_0(m_t)] . \end{aligned} \tag{4.64}$$

A comprehensive calculation can be found in A.2.3. The scalar integral  $B_0$  is defined as

$$B_0(p, m_0, m_1) := \mu^{D-4} \int \frac{d^D l}{(2\pi)^D} \frac{1}{(l^2 - m_0^2) ((p+l)^2 - m_1^2)} . \quad (4.65)$$

The Passarino-Veltman reduction is shown explicitly of the tensor integral is shown explicitly in app. A.2.1. Inserting  $\Sigma_2$  in eq. (4.61) entails

$$\begin{aligned} \Sigma_t(\hat{p}) = & \frac{m_t^2}{v^2} \cdot \left( m_t + \frac{m_t^2 - m_H^2 + p^2}{2p^2} \hat{p} \right) B_0(p, m_H, m_t) + \frac{m_t^2 \hat{p}}{2p^2 v^2} [A_0(m_H) - A_0(m_t)] \\ & + (\hat{p} - m_t) \delta Z_t - \delta m_t + \frac{m_t \delta t}{m_H^2 v} . \end{aligned} \quad (4.66)$$

Applying the first renormalization condition of eq. (4.63) yields

$$\begin{aligned}
0 &= \frac{m_t \cdot (4m_t^2 - m_H^2)}{2v^2} B_0(m_t, m_H, m_t) + \frac{m_t}{2v^2} [A_0(m_H) - A_0(m_t)] - \delta m_t + \frac{m_t \delta t}{m_H^2 v} \\
\stackrel{(A.20)}{\Leftrightarrow} \delta m_t &= \frac{m_t \cdot (4m_t^2 - m_H^2)}{2v^2} B_0(m_t, m_H, m_t) - \frac{m_t}{v^2} A_0(m_H) + \frac{2DN_c m_t^3 - m_t m_H^2}{2m_H^2 v^2} A_0(m_t) .
\end{aligned} \tag{4.67}$$

As mentioned above the counterterm  $\delta Z_t$  is not needed here, since there are no external quarks in this process.

**Higgs renormalization** An equivalent calculation is done for the Higgs propagator, to fix  $\delta Z_H$  and  $\delta m_H$ . The two-point function up to NLO reads

$$G_H(\hat{p}) = \frac{i}{p^2 - m_H^2} + \frac{i}{p^2 - m_H^2} \Sigma_2(\hat{p}) \frac{i}{p^2 - m_H^2} \quad (4.68)$$

$$+ \frac{i}{p^2 - m_H^2} \left[ (p^2 - m_H^2) \delta Z_H - \delta m_H^2 + \frac{3\delta t}{v} \right] \frac{i}{p^2 - m_H^2}.$$

A big difference to the top quark case is that here three diagrams contribute to  $\Sigma_2(\hat{p})$ .

$$\begin{aligned} \Sigma_2(\hat{p}) = & \text{---} \circ \text{---} + \text{---} \circ \text{---} + \text{---} \circ \text{---} \\ & \stackrel{[49]}{=} \sum_{\text{colors}} (-1) \mu^{-\varepsilon} \int \frac{d^D l}{(2\pi)^D} \left( -i \frac{m_t}{v} \right)^2 \text{Tr} \left[ \frac{i(\hat{l} + m_t)}{l^2 - m_t^2} \frac{i(\hat{p} + \hat{l} + m_t)}{(p+l)^2 - m_t^2} \right] \\ & + \frac{(-i c_{H^3})^2}{2} \mu^{-\varepsilon} \int \frac{d^D l}{(2\pi)^D} \frac{i^2}{(l^2 - m_H^2)((p+l)^2 - m_H^2)} + \frac{(-i c_{H^4})}{2} \mu^{-\varepsilon} \int \frac{d^D l}{(2\pi)^D} \frac{i}{l^2 - m_H^2} \\ & \stackrel{(A.21)}{=} -\frac{m_t^2}{v^2} N_c D \left[ A_0(m_t) + \frac{4m_t^2 - p^2}{2} B_0(p, m_t, m_t) \right] + \frac{c_{H^3}^2}{2} B_0(p, m_H, m_H) + \frac{c_{H^4}}{2} A_0(m_H) . \end{aligned} \quad (4.69)$$

This result can be used in the Higgs self energy

$$\begin{aligned}\Sigma_H(\hat{p}) &= \Sigma_2(\hat{p}) + \left[ (p^2 - m_H^2)\delta Z_H - \delta m_H^2 + \frac{3\delta t}{v} \right] \\ &= -\frac{m_t^2}{v^2} N_c D \left[ A_0(m_t) + \frac{4m_t^2 - p^2}{2} B_0(p, m_t, m_t) \right] + \frac{c_{H^3}^2}{2} B_0(p, m_H, m_H) + \frac{c_{H^4}}{2} A_0(m_H) \\ &\quad + (p^2 - m_H^2)\delta Z_H - \delta m_H^2 + \frac{3\delta t}{v} .\end{aligned}\tag{4.70}$$

To determine the values of  $\delta Z_H$  and  $\delta m_H$  the on-shell renormalization conditions of eq. (4.63) are used. The only necessary adjustment is the substitution of the top mass by the Higgs mass. The mass counterterm is calculated as

$$\begin{aligned}
0 &= -\frac{m_t^2}{v^2} N_c D \cdot \left[ A_0(m_t) + \frac{4m_t^2 - m_H^2}{2} B_0(m_H, m_t, m_t) \right] + \frac{c_{H^3}^2}{2} B_0(m_H, m_H, m_H) \\
&\quad + \frac{c_{H^4}}{2} A_0(m_H) - \delta m_H^2 + \frac{3\delta t}{v} \\
\stackrel{(A.26)}{\Leftrightarrow} \delta m_H^2 &= -N_c D \frac{m_t^2(4m_t^2 - m_H^2)}{2v^2} B_0(m_H, m_t, m_t) + \frac{c_{H^3}^2}{2} B_0(m_H, m_H, m_H)
\end{aligned} \tag{4.71}$$

$$+ DN_c \frac{2m_t^2}{v^2} A_0(m_t) + \left[ \frac{c_{H^4}}{2} - \frac{9m_H^2}{2v^2} \right] A_0(m_H) . \quad (4.72)$$

The wave function counterterm is computed from the condition on the derivative of  $\Sigma_H$ .

$$\begin{aligned} 0 &= -\frac{m_t^2}{v^2} N_c D \cdot \left[ \frac{4m_t^2 - m_H^2}{2} B'_0(m_H, m_t, m_t) - m_H B_0(p, m_t, m_t) \right] \\ &\quad + \frac{c_{H^3}^2}{2} B'_0(m_H, m_H, m_H) + 2m_H \delta Z_H \\ &= -\frac{m_t^2}{v^2} N_c D \cdot \frac{1}{2m_H} \left[ 2(D-2)A_0(m_t) - (4m_t^2 + m_H^2 \cdot (D-2))B_0(m_H, m_t, m_t) \right] \end{aligned} \quad (4.73)$$

$$+ \frac{c_{H^3}^2}{6m_H^3} \left[ 2(D-2)A_0(m_H) - D \cdot m_H^2 B_0(m_H, m_H, m_H) \right] + 2m_H \delta Z_H \quad (4.74)$$

$$\stackrel{(A.22)}{\Leftrightarrow} \delta Z_H = \frac{m_t^2}{v^2} N_c D \cdot \frac{1}{4m_H^2} \left[ 2(D-2)A_0(m_t) - (4m_t^2 + m_H^2 \cdot (D-2))B_0(m_H, m_t, m_t) \right] \quad (4.75)$$

$$- \frac{c_{H^3}^2}{12m_H^4} \left[ 2(D-2)A_0(m_H) - D \cdot m_H^2 B_0(m_H, m_H, m_H) \right] \quad (4.76)$$

### 4.5.3. The Renormalized Amplitude

Putting everything together, the renormalized amplitude can be constructed. The matrix element reads

$$\begin{aligned} \mathcal{M}_{\text{ren}} &= Z_g Z_H \cdot \left[ \mathcal{M}_{\text{LO}}(m_t + \delta m_t, m_H^2 + \delta m_H^2, v + \Delta v) + \mathcal{M}_{\text{NLO}}(m_t, m_H^2, v) \right] \quad (4.77) \\ &= Z_H \cdot \left[ \mathcal{M}_{\text{LO}}(m_t, m_H^2, v) + \delta m_t \frac{\partial}{\partial m_t} \mathcal{M}_{\text{LO}}(m_t, m_H^2, v) + \delta m_H^2 \frac{\partial}{\partial m_H^2} \mathcal{M}_{\text{LO}}(m_t, m_H^2, v) \right. \\ &\quad \left. + \Delta v \frac{\partial}{\partial v} \mathcal{M}_{\text{LO}}(m_t, m_H^2, v) + \mathcal{M}_{\text{NLO}}(m_t, m_H^2, v) \right] \\ &= \mathcal{M}_{\text{LO}}(m_t, m_H^2, v) + \delta m_t \frac{\partial}{\partial m_t} \mathcal{M}_{\text{LO}}(m_t, m_H^2, v) + \delta m_H^2 \frac{\partial}{\partial m_H^2} \mathcal{M}_{\text{LO}}(m_t, m_H^2, v) \\ &\quad + \Delta v \frac{\partial}{\partial v} \mathcal{M}_{\text{LO}}(m_t, m_H^2, v) + \mathcal{M}_{\text{NLO}}(m_t, m_H^2, v) + \delta Z_H \mathcal{M}_{\text{LO}}(m_t, m_H^2, v) . \end{aligned} \quad (4.78)$$

The renormalization factors  $Z_g$  and  $Z_H$  have to be included for the external legs of the contributing diagrams. In the present calculation the gluon renormalization function can be taken to be 1, since

$$Z_g = 1 + \mathcal{O}(\alpha_s) + \mathcal{O}(\alpha_s \alpha) + \dots \approx 1 . \quad (4.79)$$

The Higgs field renormalization constant  $Z_H$  can be expressed as in eq. (4.49).

De facto the counterterms are included employing a trick in *reduze*: a Higgs-Higgs vertex

and a top-top vertex with the counterterm insertion from eqs. (4.55) or (4.56) as coupling constant is added to the file `feynmanrules.yaml`. The Higgs self-interaction vertices and the Yukawa vertex are adjusted as well to incorporate the counterterm insertions of eqs. (4.57) and (4.58). Then the LO amplitude is again constructed, but this time it contains lines with the counterterm insertions. Several diagrams contain more than one counterterm insertion, which is a higher order effect. To exclude these diagrams the amplitude is expanded in the counterterm insertion vertices and the resulting sum truncated accordingly. After this procedure only diagrams containing one counterterm insertion on one internal line remain. This is identified with  $\mathcal{M}_{\text{LO}}(m_t + \delta m_t, m_H^2 + \delta m_H^2, v + \Delta v)$ . This part of the calculation is also contributed by M. Kerner.

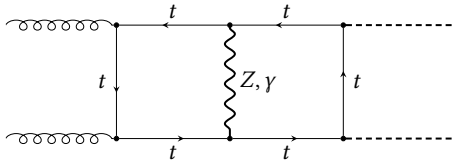
Evaluating (4.77) with a given phase-space point should then return a finite result. At present, this check still fails, i.e. the poles do not cancel each other identically. The renormalization procedure is hence understood as a work under continuing construction.



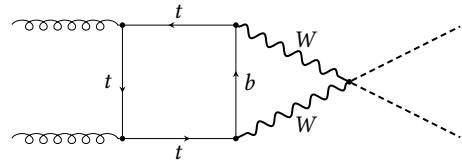
## 5. Conclusion and Directions for Further Investigations

As seen in the previous chapters, di-Higgs production is an important process to investigate the shape of the Higgs potential. Due to its small cross section, it is still mainly unexplored. The present work took first steps into direction of calculating EW NLO corrections with the full top mass dependence to this process. Some intermediate milestones to this final goal were reached: The amplitude was generated, reduced (contributed by M. Kerner) and for the first phase space points the master integrals were evaluated. Renormalization is begun, but still under development. The most pressing matter at hand is to finish this and speed up the integration routine, in order to get results distributed in a bigger phase-space volume.

A natural extension to the present work would be the inclusion of gauge bosons, requiring the calculation of diagrams similar to the ones shown in fig. 5.1. This is particular challenging, as another mass scale ( $m_W$  or  $m_Z$ ) enters the integrals.



Double box with three mass scales from  $t$  quark,  $Z$  and  $H$  boson.



The  $W$  bosons make a fourth mass scale necessary.

Figure 5.1.: Diagrams contributing to EW correction. Additional mass scales are introduced by the gauge bosons.

Another direction is the inclusion of a second quarks, especially the bottom quark. The hope is that some interesting effects might show up through the interference of diagrams which are mediated by top loops and those which are mediated by bottom loops. An investigation with POWHEG-BOX [51–53] has already been performed, based on the code in [54], which shows some unexpected structure in the tail region for varying bottom Yukawa coupling strength  $c_b$ , c.f. fig. 5.2. However, due to the large scale difference between  $m_t$  and  $m_b$  this operation is numerically challenging. A promising ansatz is the use of pySecDec with *expansion by regions*. This method expands in the small mass-scale ratio. Thus, the calculation becomes numerically stable. For some of the expected topologies this ansatz has already been tested, the results can be found in appendix A.1. Another complication is given by the necessity of computing a full symbolic reduction in order to

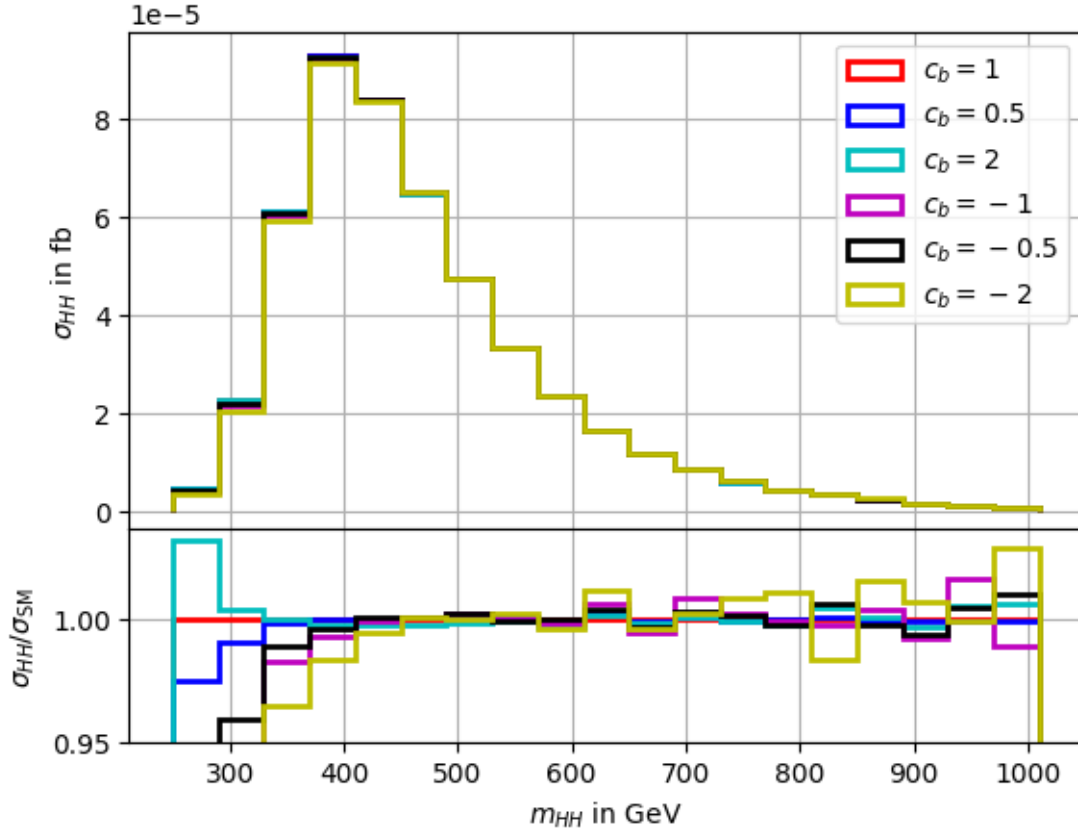


Figure 5.2.: First steps towards inclusion of bottom loops in Higgs pair production. Note the variations in the tail.

exchange the quark mass in the amplitude.

A third possibility, building directly on the calculation performed here, would be to allow for anomalous couplings in the Higgs sector. This includes anomalous Yukawa couplings as well as anomalous trilinear and quartic Higgs couplings. This is justified by the rather loose bounds on  $\lambda$  and would very probably change the distributions observed for di-Higgs production. This could be of tremendous importance for experimental physics in the coming years of HL-LHC where those distributions will be measured to a unprecedented precision.



# Bibliography

- [1] ATLAS. “Observation of an Excess of Events in the Search for the Standard Model Higgs boson with the ATLAS detector at the LHC” (July 2012).
- [2] CMS. “Observation of a new boson with a mass near 125 GeV” (2012).
- [3] F. Englert and R. Brout. “Broken Symmetry and the Mass of Gauge Vector Mesons”. *Phys. Rev. Lett.* 13 (1964). Ed. by J. C. Taylor, pp. 321–323. DOI: 10.1103/PhysRevLett.13.321.
- [4] Peter W. Higgs. “Broken symmetries, massless particles and gauge fields”. *Phys. Lett.* 12 (1964), pp. 132–133. DOI: 10.1016/0031-9163(64)91136-9.
- [5] Peter W. Higgs. “Broken Symmetries and the Masses of Gauge Bosons”. *Phys. Rev. Lett.* 13 (1964). Ed. by J. C. Taylor, pp. 508–509. DOI: 10.1103/PhysRevLett.13.508.
- [6] G. S. Guralnik, C. R. Hagen, and T. W. B. Kibble. “Global Conservation Laws and Massless Particles”. *Phys. Rev. Lett.* 13 (1964). Ed. by J. C. Taylor, pp. 585–587. DOI: 10.1103/PhysRevLett.13.585.
- [7] Peter W. Higgs. “Spontaneous Symmetry Breakdown without Massless Bosons”. *Phys. Rev.* 145 (1966), pp. 1156–1163. DOI: 10.1103/PhysRev.145.1156.
- [8] T. W. B. Kibble. “Symmetry breaking in non-Abelian gauge theories”. *Phys. Rev.* 155 (1967). Ed. by J. C. Taylor, pp. 1554–1561. DOI: 10.1103/PhysRev.155.1554.
- [9] *The Nobel Prize in Physics 2013*. Nobel Prize Outreach AB 2023. URL: <https://www.nobelprize.org/prizes/physics/2013/> (visited on 01/13/2023).
- [10] Matthew D. Schwartz. *Quantum Field Theory and the Standard Model*. Cambridge University Press, Mar. 2014. ISBN: 978-1-107-03473-0.
- [11] P.A. Zyla et al. “Review of Particle Physics”. *PTEP* 2020.8 (2020). and 2021 update, p. 083C01. DOI: 10.1093/ptep/ptaa104.
- [12] J. Goldstone. “Field Theories with “Superconductor” solutions”. *Il Nuovo Cimento* 19.1 (Jan. 1, 1961). DOI: 10.1007/BF02812722.
- [13] The CMS Collaboration. “A portrait of the Higgs boson by the CMS experiment ten years after the discovery”. *Nature* 607 (7917 July 1, 2022), pp. 60–68. DOI: 10.1038/s41586-022-04892-x.
- [14] “Constraining the Higgs boson self-coupling from single- and double-Higgs production with the ATLAS detector using  $pp$  collisions at  $\sqrt{s} = 13$  TeV” (Nov. 2022). arXiv: 2211.01216 [hep-ex].
- [15] M. Cepeda et al. “Report from Working Group 2: Higgs Physics at the HL-LHC and HE-LHC”. *CERN Yellow Rep. Monogr.* 7 (2019). Ed. by Andrea Dainese et al., pp. 221–584. DOI: 10.23731/CYRM-2019-007.221. arXiv: 1902.00134 [hep-ph].

- [16] J. Alison et al. “Higgs boson potential at colliders: Status and perspectives”. *Rev. Phys.* 5 (2020). Ed. by Biagio Di Micco et al., p. 100045. DOI: 10.1016/j.revip.2020.100045. arXiv: 1910.00012 [hep-ph].
- [17] Margarete Mühlleitner, Johannes Schlenk, and Michael Spira. “Top-Yukawa-induced corrections to Higgs pair production”. *JHEP* 10 (2022), p. 185. DOI: 10.1007/JHEP10(2022)185. arXiv: 2207.02524 [hep-ph].
- [18] S. Borowka et al. “Higgs Boson Pair Production in Gluon Fusion at Next-to-Leading Order with Full Top-Quark Mass Dependence”. *Phys. Rev. Lett.* 117.1 (2016). [Erratum: *Phys.Rev.Lett.* 117, 079901 (2016)], p. 012001. DOI: 10.1103/PhysRevLett.117.079901. arXiv: 1604.06447 [hep-ph].
- [19] S. Borowka et al. “Full top quark mass dependence in Higgs boson pair production at NLO”. *JHEP* 10 (2016), p. 107. DOI: 10.1007/JHEP10(2016)107. arXiv: 1608.04798 [hep-ph].
- [20] Julien Baglio et al. “Gluon fusion into Higgs pairs at NLO QCD and the top mass scheme”. *Eur. Phys. J. C* 79.6 (2019), p. 459. DOI: 10.1140/epjc/s10052-019-6973-3. arXiv: 1811.05692 [hep-ph].
- [21] J. Baglio et al. “Higgs-Pair Production via Gluon Fusion at Hadron Colliders: NLO QCD Corrections”. *JHEP* 04 (2020), p. 181. DOI: 10.1007/JHEP04(2020)181. arXiv: 2003.03227 [hep-ph].
- [22] Daniel de Florian and Javier Mazzitelli. “Two-loop virtual corrections to Higgs pair production”. *Phys. Lett. B* 724 (2013), pp. 306–309. DOI: 10.1016/j.physletb.2013.06.046. arXiv: 1305.5206 [hep-ph].
- [23] Daniel de Florian and Javier Mazzitelli. “Higgs Boson Pair Production at Next-to-Next-to-Leading Order in QCD”. *Phys. Rev. Lett.* 111 (2013), p. 201801. DOI: 10.1103/PhysRevLett.111.201801. arXiv: 1309.6594 [hep-ph].
- [24] Jonathan Grigo, Kirill Melnikov, and Matthias Steinhauser. “Virtual corrections to Higgs boson pair production in the large top quark mass limit”. *Nucl. Phys. B* 888 (2014), pp. 17–29. DOI: 10.1016/j.nuclphysb.2014.09.003. arXiv: 1408.2422 [hep-ph].
- [25] Jonathan Grigo, Jens Hoff, and Matthias Steinhauser. “Higgs boson pair production: top quark mass effects at NLO and NNLO”. *Nucl. Phys. B* 900 (2015), pp. 412–430. DOI: 10.1016/j.nuclphysb.2015.09.012. arXiv: 1508.00909 [hep-ph].
- [26] Daniel de Florian et al. “Differential Higgs Boson Pair Production at Next-to-Next-to-Leading Order in QCD”. *JHEP* 09 (2016), p. 151. DOI: 10.1007/JHEP09(2016)151. arXiv: 1606.09519 [hep-ph].
- [27] Long-Bin Chen et al. “Higgs boson pair production via gluon fusion at N<sup>3</sup>LO in QCD”. *Phys. Lett. B* 803 (2020), p. 135292. DOI: 10.1016/j.physletb.2020.135292. arXiv: 1909.06808 [hep-ph].
- [28] Long-Bin Chen et al. “The gluon-fusion production of Higgs boson pair: N<sup>3</sup>LO QCD corrections and top-quark mass effects”. *JHEP* 03 (2020), p. 072. DOI: 10.1007/JHEP03(2020)072. arXiv: 1912.13001 [hep-ph].

- 
- [29] S. Dawson, S. Dittmaier, and M. Spira. “Neutral Higgs boson pair production at hadron colliders: QCD corrections”. *Phys. Rev. D* 58 (1998), p. 115012. DOI: 10.1103/PhysRevD.58.115012. arXiv: hep-ph/9805244.
  - [30] F. Maltoni, E. Vryonidou, and M. Zaro. “Top-quark mass effects in double and triple Higgs production in gluon-gluon fusion at NLO”. *JHEP* 11 (2014), p. 079. DOI: 10.1007/JHEP11(2014)079. arXiv: 1408.6542 [hep-ph].
  - [31] Joshua Davies et al. “Higgs boson contribution to the leading two-loop Yukawa corrections to  $gg \rightarrow HH$ ”. *JHEP* 08 (2022), p. 259. DOI: 10.1007/JHEP08(2022)259. arXiv: 2207.02587 [hep-ph].
  - [32] E. W. Nigel Glover and J. J. van der Bij. “HIGGS BOSON PAIR PRODUCTION VIA GLUON FUSION”. *Nucl. Phys. B* 309 (1988), pp. 282–294. DOI: 10.1016/0550-3213(88)90083-1.
  - [33] Paulo Nogueira. “Automatic Feynman graph generation”. *J. Comput. Phys.* 105 (1993), pp. 279–289. DOI: 10.1006/jcph.1993.1074.
  - [34] V. Magerya. *ALIBRARY: all the glue for computing multiloop amplitudes in QCD and beyond*. 2022. URL: <https://github.com/magv/alibrary>.
  - [35] Jonas Klappert et al. “Integral reduction with Kira 2.0 and finite field methods”. *Comput. Phys. Commun.* 266 (2021), p. 108024. DOI: 10.1016/j.cpc.2021.108024. arXiv: 2008.06494 [hep-ph].
  - [36] Philipp Maierhöfer, Johann Usovitsch, and Peter Uwer. “Kira—A Feynman integral reduction program”. *Comput. Phys. Commun.* 230 (2018), pp. 99–112. DOI: 10.1016/j.cpc.2018.04.012. arXiv: 1705.05610 [hep-ph].
  - [37] R. H. Lewis. *Computer Algebra System Fermat*. URL: <https://home.bway.net/lewis>.
  - [38] A. von Manteuffel and C. Studerus. “Reduze 2 - Distributed Feynman Integral Reduction” (Jan. 2012). arXiv: 1201.4330 [hep-ph].
  - [39] S. Laporta. “High precision calculation of multiloop Feynman integrals by difference equations”. *Int. J. Mod. Phys. A* 15 (2000), pp. 5087–5159. DOI: 10.1142/S0217751X00002159. arXiv: hep-ph/0102033.
  - [40] Gudrun Heinrich. “Collider Physics at the Precision Frontier”. *Phys. Rept.* 922 (2021), pp. 1–69. DOI: 10.1016/j.physrep.2021.03.006. arXiv: 2009.00516 [hep-ph].
  - [41] S. Borowka et al. “pySecDec: a toolbox for the numerical evaluation of multi-scale integrals”. *Comput. Phys. Commun.* 222 (2018), pp. 313–326. DOI: 10.1016/j.cpc.2017.09.015. arXiv: 1703.09692 [hep-ph].
  - [42] S. Borowka et al. “A GPU compatible quasi-Monte Carlo integrator interfaced to pySecDec”. *Comput. Phys. Commun.* 240 (2019), pp. 120–137. DOI: 10.1016/j.cpc.2019.02.015. arXiv: 1811.11720 [physics.comp-ph].
  - [43] G. Heinrich et al. “Expansion by regions with pySecDec”. *Comput. Phys. Commun.* 273 (2022), p. 108267. DOI: 10.1016/j.cpc.2021.108267. arXiv: 2108.10807 [hep-ph].

- [44] T. Binoth and G. Heinrich. “An automatized algorithm to compute infrared divergent multiloop integrals”. *Nucl. Phys. B* 585 (2000), pp. 741–759. DOI: 10.1016/S0550-3213(00)00429-6. arXiv: hep-ph/0004013.
- [45] Gudrun Heinrich. “Sector Decomposition”. *Int. J. Mod. Phys. A* 23 (2008), pp. 1457–1486. DOI: 10.1142/S0217751X08040263. arXiv: 0803.4177 [hep-ph].
- [46] S. Borowka et al. “SecDec-3.0: numerical evaluation of multi-scale integrals beyond one loop”. *Comput. Phys. Commun.* 196 (2015), pp. 470–491. DOI: 10.1016/j.cpc.2015.05.022. arXiv: 1502.06595 [hep-ph].
- [47] *Electroweak Radiative Corrections for Collider Physics*. Apr. 9, 2020. DOI: 10.48550/arXiv.1912.06823.
- [48] F. Jegerlehner J. Fleischer. “Radiative corrections to Higgs-boson decays in the Weinberg-Salam model”. *Physical Review D* 23.9 (May 1, 1981).
- [49] Jorge C. Romao and Joao P. Silva. “A resource for signs and Feynman diagrams of the Standard Model”. *Int. J. Mod. Phys. A* 27 (2012), p. 1230025. DOI: 10.1142/S0217751X12300256. arXiv: 1209.6213 [hep-ph].
- [50] R. Keith Ellis and Giulia Zanderighi. “Scalar one-loop integrals for QCD”. *JHEP* 02 (2008), p. 002. DOI: 10.1088/1126-6708/2008/02/002. arXiv: 0712.1851 [hep-ph].
- [51] Paolo Nason. “A New method for combining NLO QCD with shower Monte Carlo algorithms”. *JHEP* 11 (2004), p. 040. DOI: 10.1088/1126-6708/2004/11/040. arXiv: hep-ph/0409146.
- [52] Stefano Frixione, Paolo Nason, and Carlo Oleari. “Matching NLO QCD computations with Parton Shower simulations: the POWHEG method”. *JHEP* 11 (2007), p. 070. DOI: 10.1088/1126-6708/2007/11/070. arXiv: 0709.2092 [hep-ph].
- [53] Simone Alioli et al. “A general framework for implementing NLO calculations in shower Monte Carlo programs: the POWHEG BOX”. *JHEP* 06 (2010), p. 043. DOI: 10.1007/JHEP06(2010)043. arXiv: 1002.2581 [hep-ph].
- [54] G. Heinrich et al. “Probing the trilinear Higgs boson coupling in di-Higgs production at NLO QCD including parton shower effects”. *JHEP* 06 (2019), p. 066. DOI: 10.1007/JHEP06(2019)066. arXiv: 1903.08137 [hep-ph].

# A. Appendix

## A.1. Integrals with Bottom Quark Loops

Table A.1.: Values for some sectors of the families used for the reduction, where the top quark is exchanged for a bottom quark. The column “dim.” shows the dimensionality of the integral,  $\mathcal{O}$  the order in  $\varepsilon$ , the columns labelled with the  $\sigma$  contain the numerical uncertainty.

Family	Sector	Quark	dim.	$\mathcal{O}$	Re	Im	Re( $\sigma$ )	Im( $\sigma$ )	Fig.
F1	254	top	6	$\varepsilon^0$	-0.0819	-0.0075	0.0006	0.0005	A.1a
		bottom	6	$\varepsilon^0$	0.1703	-0.0745	0.0007	0.0008	
	439	top	6	$\varepsilon^0$	-0.0363	-0.0005	0.00017	0.00018	A.1b
		bottom	6	$\varepsilon^0$	-0.250	-0.339	0.0017	0.002	
	445	top	4	$\varepsilon^0$	-0.0408	0.0895	0.0004	0.0004	A.1c
		top	4	$\varepsilon^{-1}$	0.0490	0.0290	0.00014	0.00013	
F2	254	top	6	$\varepsilon^0$	-0.0352	-0.0004	0.00016	0.00017	A.1d
		bottom	6	$\varepsilon^0$	-0.355	-0.222	0.0017	0.0019	
F3	190	top	6	$\varepsilon^0$	-0.111	-0.150	0.0010	0.0011	A.1e
		bottom	6	$\varepsilon^0$	0.0911	-0.0980	0.0009	0.0009	
F4	381	top	6	$\varepsilon^0$	-0.0965	-0.0519	0.0007	0.0007	A.1f
		bottom	6	$\varepsilon^0$	0.094	-0.203	0.0012	0.0013	
F6h	239	top	6	$\varepsilon^0$	-0.0573	-0.0287	0.0003	0.0003	A.1g
		bottom	6	$\varepsilon^0$	-0.059	-0.262	0.0012	0.0013	
F7h	439	top	6	$\varepsilon^0$	-0.0308	-0.0004	0.00015	0.00016	A.1h
		bottom	6	$\varepsilon^0$	-0.222	-0.167	0.0011	0.0012	
	445	top	6	$\varepsilon^0$	-0.0496	-0.0024	0.0003	0.0002	A.1i
		bottom	6	$\varepsilon^0$	0.0677	-0.1923	0.0009	0.001	

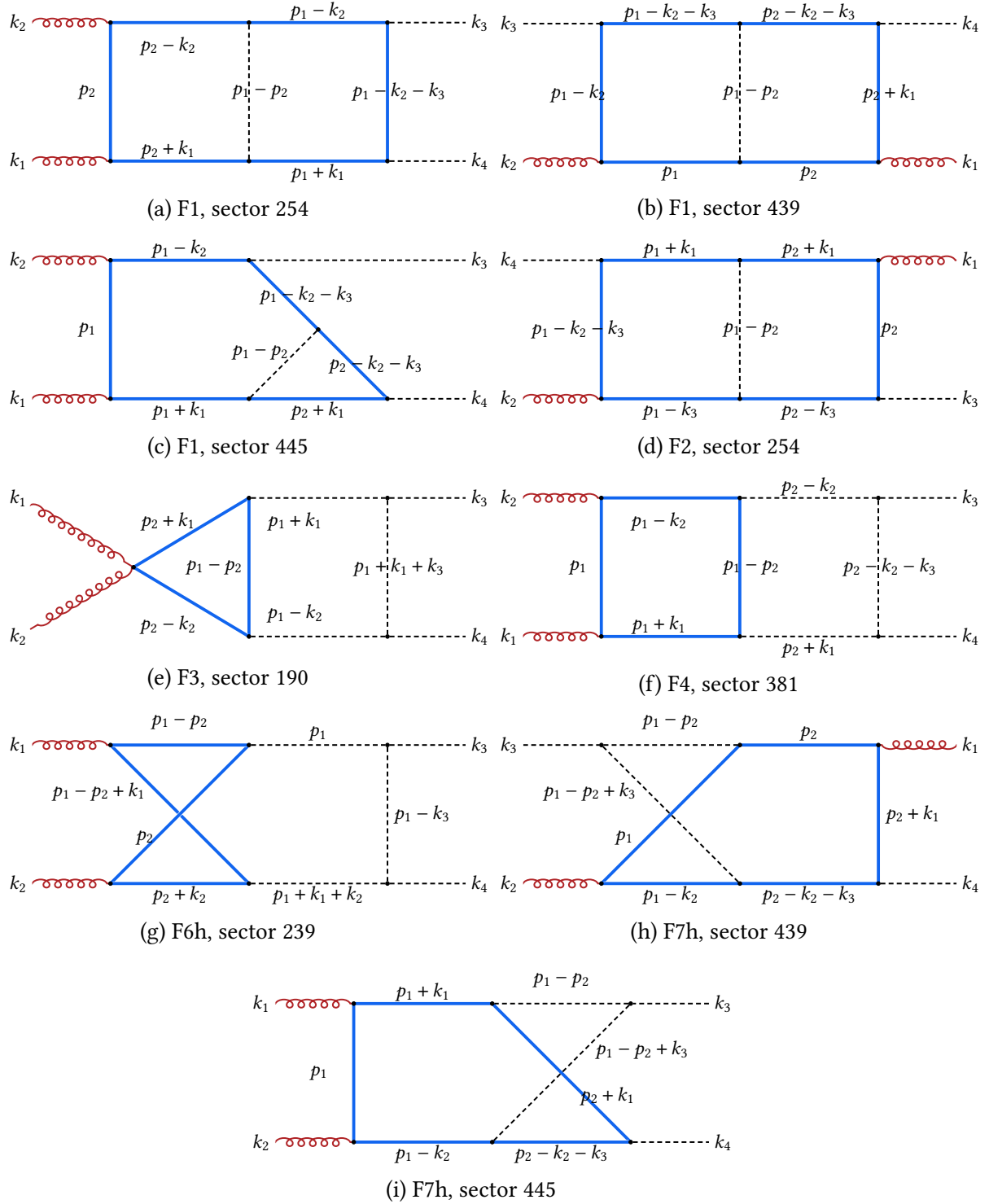


Figure A.1.: The diagrams, whose values are given in tab. A.1. The lower three are non-planar.

## A.2. Scalar Integrals and Passarino-Veltman Reduction

In the performed 1-loop calculation scalar integrals turn up. Their integrand is a fraction, whose denominator is a product of objects like  $(P^2 - m^2)$ .  $P$  can be any linear combination of external and loop momenta, and  $m$  a mass. The numerator can depend on the loop momenta, such that the integral itself carries a Lorentz structure. This is called a tensor integral where the rank of the tensor equals the number of loop momenta in the numerator. Tensor integrals can be reduced to scalar integrals using Passarino-Veltman reduction, as shown in sec. A.2.1. In sec. A.2.2 the derivation and the following reduction of a scalar integral is shown. Finally, sec. A.2.3 applies the results to some calculations required in sec. 4.5.

As already seen in eq. (4.44) and (4.65) the notation used here for the scalar integrals is the following:

$$A_0(m_0) = \int \frac{d^4 l}{(2\pi)^4} \frac{1}{(l^2 - m_0^2)} \quad (\text{A.1})$$

$$B_0(p_1, m_0, m_1) = \int \frac{d^4 l}{(2\pi)^4} \frac{1}{(l^2 - m_0^2)((l + p_1)^2 - m_1^2)} \quad (\text{A.2})$$

$$C_0(p_1, p_2, m_0, m_1, m_2) = \int \frac{d^4 l}{(2\pi)^4} \frac{1}{(l^2 - m_0^2)((l + p_1)^2 - m_1^2)((l + p_1 + p_2)^2 - m_2^2)} \quad (\text{A.3})$$

Due to the length of the expressions the arguments are often omitted, especially in the calculations below. Often, the switch to  $D$  dimensions instead of the given 4 is assumed. To conserve the correct mass dimension, this requires the introduction of a mass correction factor  $\mu$ , e.g.

$$B_0 = \mu^{4-D} \int \frac{d^D l}{(2\pi)^D} \frac{1}{(l^2 - m_0^2)((l + p_1)^2 - m_1^2)} . \quad (\text{A.4})$$

Tensor integrals carry the according Lorentz indices additionally to the integer indices. The abbreviation

$$D_i = \left( l + \sum_1^i p_i \right)^2 - m_i^2 \quad (\text{A.5})$$

in the denominators of the integrands is frequently employed. Any arguments of scalar functions are usually omitted, unless this introduces ambiguities.

The integrals can be evaluated as an expansion in  $\varepsilon$ . A list of many of them can be found in [50].

### A.2.1. Tensor integral reduction

In the course of the present calculations one tensor integral is relevant. It is defined as

$$B_0^\mu(p, m_0, m_1) = \mu^{4-D} \int \frac{d^D l}{(2\pi)^D} \frac{l^\mu}{D_0 D_1} . \quad (\text{A.6})$$

This integral's Lorentz structure can only be written as

$$B_0^\mu = c p^\mu. \quad (\text{A.7})$$

Projecting onto  $p_\mu$  yields all necessary relations.

$$\begin{aligned} p_\mu B_0^\mu &= c p^2 = \mu^{4-D} \int \frac{d^D l}{(2\pi)^D} \frac{p \cdot l}{D_0 D_1} = \mu^{4-D} \int \frac{d^D l}{(2\pi)^D} \frac{D_1 - D_0 - p^2 + m_1^2 - m_0^2}{2 D_0 D_1} \\ &= \frac{\mu^{4-D}}{2} \int \frac{d^D l}{(2\pi)^D} \left[ \frac{1}{D_0} - \frac{1}{D_1} + \frac{m_1^2 - m_0^2 - p^2}{D_0 D_1} \right] = \frac{A_0(m_0) - A_0(m_1)}{2} + \frac{m_1^2 - m_0^2 - p^2}{2} B_0 \end{aligned} \quad (\text{A.8})$$

The final result for  $B^\mu$  is

$$B_0^\mu(p, m_0, m_1) = \frac{p^\mu}{2p^2} [A_0(m_0) - A_0(m_1) + (m_1^2 - m_0^2 - p^2) B_0]. \quad (\text{A.9})$$

### A.2.2. Derivative of the Scalar Functions

One of the conditions for the on-shell renormalization scheme includes a derivative. Here the derivative of  $B_0$  is needed.

$$\begin{aligned} \frac{\partial}{\partial \hat{p}} B_0 &= \mu^{4-D} \int \frac{d^D l}{(2\pi)^D} \frac{\frac{\partial}{\partial \hat{p}} \left( (\hat{l} + \hat{p})^2 - m_1^2 \right)^{-1}}{(l^2 - m_0^2)} = \mu^{4-D} \int \frac{d^D l}{(2\pi)^D} \frac{-2(\hat{l} + \hat{p})}{(l^2 - m_0^2) ((l + p)^2 - m_1^2)^2} \\ &= -2\mu^{4-D} \int \frac{d^D l}{(2\pi)^D} \frac{(\hat{l} + \hat{p})}{D_0 D_1^2} = -2 \left[ \hat{p} B_{12} + \gamma_\mu \mu^{4-D} \int \frac{d^D l}{(2\pi)^D} \frac{l^\mu}{D_0 D_1^2} \right] = -2 [\hat{p} B_{12} + \gamma_\mu B_{12}^\mu] \\ &= -2 \left[ \hat{p} B_{12} + \frac{\hat{p}}{2p^2} \left( B_0 - A_2 - (p^2 + m_0^2 - m_1^2) \cdot B_{12} \right) \right] \\ &= \frac{\hat{p}}{p^2} [A_2 - B_0 - (p^2 + m_1^2 - m_0^2) \cdot B_{12}] \end{aligned} \quad (\text{A.10})$$

Scalar functions with more than one index contain dots. The multiple indices represent the respective propagator powers. In this formalism  $B_0 \equiv B_{11}$  and  $A_0 \equiv B_{10}$ . Similar to eq. (A.9) also the dotted tensor integral is reduced to

$$B_{12}^\mu = \frac{p^\mu}{2p^2} [B_0 - A_2 + (m_1^2 - m_0^2 - p^2) B_{12}] \quad (\text{A.11})$$

in the second to last step. Using IBP reduction the dotted scalar functions can again be expressed by their simpler siblings.

$$\begin{aligned} 0 &= \mu^{4-D} \int \frac{d^D l}{(2\pi)^D} \frac{d}{dl^\mu} \frac{l^\nu g_\nu^\mu}{D_0 D_1} = \mu^{4-D} \int \frac{d^D l}{(2\pi)^D} \left[ \frac{D}{D_0 D_1} + l^\mu \frac{-2l_\mu}{D_0^2 D_1} + l^\mu \frac{-2(l_\mu + p_\mu)}{D_0 D_1^2} \right] \\ &= D \cdot B_0 - 2 \cdot \mu^{4-D} \int \frac{d^D l}{(2\pi)^D} \left[ \frac{l^2 - m_0^2 + m_0^2}{D_0^2 D_1} + \frac{l^2 - m_0^2 + m_0^2 + l \cdot p}{D_0 D_1^2} \right] \end{aligned}$$



$$\begin{aligned}
 &= (D-2) \cdot B_0 - 2m_0^2 \cdot B_{21} - 2 \cdot B_{02} - 2m_0^2 \cdot B_{12} - 2\mu^{4-D} \int \frac{d^D l}{(2\pi)^D} \frac{l \cdot p}{D_0 D_1^2} \\
 &= (D-2) \cdot B_0 - 2m_0^2 \cdot B_{21} - 2 \cdot B_{02} - 2m_0^2 \cdot B_{12} - \mu^{4-D} \int \frac{d^D l}{(2\pi)^D} \frac{D_1 - D_0 - m_0^2 - p^2 + m_1^2}{D_0 D_1^2} \\
 &= (D-2) \cdot B_0 - 2m_0^2 \cdot B_{21} - 2 \cdot B_{02} - 2m_0^2 \cdot B_{12} - B_0 + B_{02} + (m_0^2 + p^2 - m_1^2) B_{12} \\
 &= (D-3) \cdot B_0 - 2m_0^2 \cdot B_{21} - B_{02} + (p^2 - m_1^2 + m_0^2) B_{12} \tag{A.12}
 \end{aligned}$$

Before an equation for  $B_{12}$  is found, first  $B_{02} = B_{20} = A_2$  has to be reduced, following the same steps.

$$\begin{aligned}
 0 &= \mu^{4-D} \int \frac{d^D l}{(2\pi)^D} \frac{d}{dl^\mu} \frac{l^\nu g^\mu_\nu}{D_0} = \mu^{4-D} \int \frac{d^D l}{(2\pi)^D} \left[ \frac{D}{D_0} + l^\mu \frac{-2l_\mu}{D_0^2} \right] = D \cdot A_0 - 2\mu^{4-D} \int \frac{d^D l}{(2\pi)^D} \frac{l^2 - m_0^2 + m_0^2}{D_0^2} \\
 &= (D-2) \cdot A_0 - 2m_0^2 A_2 \tag{A.13}
 \end{aligned}$$

So this yields

$$A_2 = \frac{D-2}{2m_0^2} A_0 . \tag{A.14}$$

Inserted in eq. (A.12) this entails

$$0 = (D-3) \cdot B_0 - 2m_0^2 \cdot B_{21} + \frac{2-D}{2m_0^2} A_0 + (p^2 - m_1^2 - m_0^2) B_{12} . \tag{A.15}$$

In the special case of  $m_0 \equiv m_1 =: m$  it is further possible to use

$$\begin{aligned}
 B_{12}(p, m, m) &= \int \frac{d^4 l}{(2\pi)^4} \frac{1}{(l^2 - m^2)((l+p)^2 - m^2)^2} \stackrel{l \rightarrow l-p}{=} \int \frac{d^4 l}{(2\pi)^4} \frac{1}{((l-p)^2 - m^2)(l^2 - m^2)^2} \\
 &\stackrel{l^\nu \rightarrow -l^\nu}{=} \int \frac{d^4 l}{(2\pi)^4} \frac{1}{((l+p)^2 - m^2)(l^2 - m^2)^2} = B_{21}(p, m, m) , \tag{A.16}
 \end{aligned}$$

and thus simplify above eq. (A.15) further to obtain

$$B_{12} = \frac{D-3}{4m^2 - s} \cdot B_0 + \frac{2-D}{2m^2(4m^2 - s)} A_0 . \tag{A.17}$$

The relation  $s = p^2$  is used. Upon returning to the original problem, but now with identical masses  $m_0$  and  $m_1$ , from eq. (A.10), the derivative reveals itself to be

$$\begin{aligned}
 \frac{\partial}{\partial \hat{p}} B_0 &= \frac{\hat{p}}{p^2} \left[ \frac{D-2}{2m^2} A_0 - B_0 - s \cdot \left( \frac{D-3}{4m^2 - s} \cdot B_0 + \frac{2-D}{2m^2(4m^2 - s)} A_0 \right) \right] \\
 &= \frac{\hat{p}}{(4m^2 - s)s} [2(D-2)A_0 - (4m^2 + s \cdot (D-4)) \cdot B_0] \tag{A.18}
 \end{aligned}$$

### A.2.3. Comprehensive Calculations from the Renormalization

Top quark self energy.

$$\begin{aligned}
 \Sigma_2(\hat{p}) &= \left(-i\frac{m_t}{v}\right)^2 \mu^{4-D} \int \frac{d^D l}{(2\pi)^D} \frac{i(\hat{p} + \hat{l} + m_t)}{(p+l)^2 - m_t^2} \cdot \frac{i}{l^2 - m_H^2} \\
 &= \frac{m_t^2}{v^2} \cdot \left[ (\hat{p} + m_t) B_0(p, m_H, m_t) + \mu^{4-D} \gamma_\mu \int \frac{d^D l}{(2\pi)^D} \frac{l^\mu}{(l^2 - m_H^2)((p+l)^2 - m_t^2)} \right] \\
 &= \frac{m_t^2}{v^2} \cdot \left( m_t + \frac{m_t^2 - m_H^2 + p^2}{2p^2} \hat{p} \right) B_0(p, m_H, m_t) + \frac{m_t^2 \hat{p}}{2p^2 v^2} [A_0(m_H) - A_0(m_t)] .
 \end{aligned} \tag{A.19}$$

Top quark mass renormalization counterterm.

$$\begin{aligned}
 0 &= \frac{m_t \cdot (4m_t^2 - m_H^2)}{2v^2} B_0(m_t, m_H, m_t) + \frac{m_t}{2v^2} [A_0(m_H) - A_0(m_t)] - \delta m_t + \frac{m_t \delta t}{m_H^2 v} \\
 \Leftrightarrow \delta m_t &= \frac{m_t \cdot (4m_t^2 - m_H^2)}{2v^2} B_0(m_t, m_H, m_t) - \frac{m_t}{v^2} A_0(m_H) + \frac{2DN_c m_t^3 - m_t m_H^2}{2m_H^2 v^2} A_0(m_t) .
 \end{aligned} \tag{A.20}$$

Higgs self energy.

$$\begin{aligned}
 \Sigma_2(\hat{p}) &= \sum_{\text{colors}} (-1) \mu^{4-D} \int \frac{d^D l}{(2\pi)^D} \left(-i\frac{m_t}{v}\right)^2 \text{Tr} \left[ \frac{i(\hat{l} + m_t)}{l^2 - m_t^2} \frac{i(\hat{p} + \hat{l} + m_t)}{(p+l)^2 - m_t^2} \right] \\
 &\quad + \frac{(-ic_{H^3})^2}{2} \mu^{4-D} \int \frac{d^D l}{(2\pi)^D} \frac{i^2}{(l^2 - m_H^2)((p+l)^2 - m_H^2)} + \frac{(-ic_{H^4})}{2} \mu^{4-D} \int \frac{d^D l}{(2\pi)^D} \frac{i}{l^2 - m_H^2} \\
 &= -\frac{m_t^2}{v^2} N_c \mu^{4-D} \int \frac{d^D l}{(2\pi)^D} \frac{\text{Tr}[p \cdot l + m_t^2 + l^2]}{(l^2 - m_t^2)((p+l)^2 - m_t^2)} \\
 &\quad + \frac{(-ic_{H^3})^2}{2} \mu^{4-D} \int \frac{d^D l}{(2\pi)^D} \frac{i^2}{(l^2 - m_H^2)((p+l)^2 - m_H^2)} + \frac{(-ic_{H^4})}{2} \mu^{4-D} \int \frac{d^D l}{(2\pi)^D} \frac{i}{l^2 - m_H^2} \\
 &= -\frac{m_t^2}{v^2} N_c D [A_0(m_t) + 2m_t^2 B_0(p, m_t, m_t) + p_\mu B_0^\mu(p, m_t, m_t)] \\
 &\quad + \frac{(-ic_{H^3})^2}{2} \mu^{4-D} \int \frac{d^D l}{(2\pi)^D} \frac{i^2}{(l^2 - m_H^2)((p+l)^2 - m_H^2)} + \frac{(-ic_{H^4})}{2} \mu^{4-D} \int \frac{d^D l}{(2\pi)^D} \frac{i}{l^2 - m_H^2} \\
 &= -\frac{m_t^2}{v^2} N_c D \left[ A_0(m_t) + \frac{4m_t^2 - p^2}{2} B_0(p, m_t, m_t) \right] + \frac{c_{H^3}^2}{2} B_0(p, m_H, m_H) + \frac{c_{H^4}}{2} A_0(m_H) .
 \end{aligned} \tag{A.21}$$

Higgs wave function renormalization counterterm.

$$0 = -\frac{m_t^2}{v^2} N_c D \cdot \left[ \frac{4m_t^2 - m_H^2}{2} B_0'(m_H, m_t, m_t) - m_H B_0(m_H, m_t, m_t) \right]$$

$$\begin{aligned}
 & + \frac{c_{H^3}^2}{2} B'_0(m_H, m_H, m_H) + 2m_H \delta Z_H \\
 & = - \frac{m_t^2}{v^2} N_c D \cdot \left[ \frac{4m_t^2 - m_H^2}{2} \frac{m_H}{(4m_t^2 - s)s} [2(D-2)A_0 - (4m_t^2 + s \cdot (D-4)) \cdot B_0] \right. \quad (A.22) \\
 & \quad \left. - m_H B_0(m_H, m_t, m_t) \right] + \frac{c_{H^3}^2}{2} \frac{m_H}{(4m_H^2 - s)s} [2(D-2)A_0 - (4m_H^2 + s \cdot (D-4)) \cdot B_0]
 \end{aligned}$$

$$(A.23)$$

$$\begin{aligned}
 & + 2m_H \delta Z_H \\
 & = - \frac{m_t^2}{v^2} N_c D \cdot \frac{1}{2m_H} [2(D-2)A_0(m_t) - (4m_t^2 + m_H^2 \cdot (D-2))B_0(m_H, m_t, m_t)] \quad (A.24)
 \end{aligned}$$

$$+ \frac{c_{H^3}^2}{6m_H^3} [2(D-2)A_0(m_H) - D \cdot m_H^2 B_0(m_H, m_H, m_H)] + 2m_H \delta Z_H \quad (A.25)$$

Higgs mass renormalization counterterm.

$$\begin{aligned}
 0 & = - \frac{m_t^2}{v^2} N_c D \cdot \left[ A_0(m_t) + \frac{4m_t^2 - m_H^2}{2} B_0(m_H, m_t, m_t) \right] + \frac{c_{H^3}^2}{2} B_0(m_H, m_H, m_H) \\
 & + \frac{c_{H^4}}{2} A_0(m_H) - \delta m_H^2 + \frac{3\delta t}{v} \quad (A.26)
 \end{aligned}$$

$$\begin{aligned}
 & = - \frac{m_t^2}{v^2} N_c D \cdot \left[ A_0(m_t) + \frac{4m_t^2 - m_H^2}{2} B_0(m_H, m_t, m_t) \right] + \frac{c_{H^3}^2}{2} B_0(m_H, m_H, m_H) \\
 & + \frac{c_{H^4}}{2} A_0(m_H) - \delta m_H^2 + \frac{3}{v} \left[ D N_c \frac{m_t^2}{v} A_0(m_t) - \frac{3m_H^2}{2v} A_0(m_H) \right] \quad (A.27)
 \end{aligned}$$

$$\begin{aligned}
 & = - N_c D \frac{m_t^2(4m_t^2 - m_H^2)}{2v^2} B_0(m_H, m_t, m_t) + \frac{c_{H^3}^2}{2} B_0(m_H, m_H, m_H) \\
 & - \delta m_H^2 + \left[ D N_c \frac{3m_t^2}{v^2} - \frac{m_t^2}{v^2} N_c D \right] A_0(m_t) + \left[ \frac{c_{H^4}}{2} - \frac{9m_H^2}{2v^2} \right] A_0(m_H) \quad (A.28)
 \end{aligned}$$

$$\begin{aligned}
 \Leftrightarrow \quad \delta m_H^2 & = - N_c D \frac{m_t^2(4m_t^2 - m_H^2)}{2v^2} B_0(m_H, m_t, m_t) + \frac{c_{H^3}^2}{2} B_0(m_H, m_H, m_H) \\
 & + D N_c \frac{2m_t^2}{v^2} A_0(m_t) + \left[ \frac{c_{H^4}}{2} - \frac{9m_H^2}{2v^2} \right] A_0(m_H) \quad (A.29)
 \end{aligned}$$